UTTAC-78, 2009

UTTAC

ANNUAL REPORT 2008

TANDEM ACCELERATOR COMPLEX
Research Facility Center for Science and Technology
University of Tsukuba

http://www.tac.tsukuba.ac.jp/

UTTAC

ANNUAL REPORT 2008

April 1, 2008 – March 31, 2009

UTTAC-78 2009

Executive Editor: Hiroshi Kudo
Editors: Yoshihiro Yamato, Daiichiro Sekiba, Kimikazu Sasa, Tetsuro Komatsubara

---

UTTAC is a series of issues, which include annual reports of
Tandem Accelerator Complex, Research Facility Center
for Science and Technology, University of Tsukuba.
The issues may also include irregular reports written by English.

Tandem Accelerator Complex, Research Facility Center for Science and Technology,
University of Tsukuba
Tennodai 1-1-1, Tsukuba, Ibaraki 305-8577, Japan

http://www.tac.tsukuba.ac.jp/
annual@tac.tsukuba.ac.jp

PREFACE

This annual report covers researches carried out at University of Tsukuba Tandem Accelerator Complex (UTTAC) during the fiscal year 2008 (1 April 2008 ~ 31 March 2009). The topics include not only accelerator-based researches using the 12UD Pelletron and 1 MV Tandetron accelerators, but also closely related researches to UTTAC.

August 15, 2009
Editors

CONTENTS

1.

ACCELERATOR AND EXPERIMENTAL FACILITIES

1.1 Accelerator operation 2008

K. Sasa, S. Ishii, H. Kimura, H. Oshima, Y. Tajima, T. Takahashi, Y. Yamato,
T. Komatsubara, D. Sekiba and H. Kudo.

The total service time of the UTTAC multi-tandem accelerator facilities was 145 days (3,480 hours) in the fiscal year 2008. 24.8 % (864 hours) of the total service time was used by industrial users, under the project "Open Advanced Facilities Initiative for Innovation (strategic use by industry)", which was supported financially by the Ministry of Education, Culture, Sports, Science and Technology since 2007.

The 12UD Pelletron tandem accelerator

The operating time and the experimental beam time of the 12UD Pelletron tandem accelerator were 1605.5 and 1177.4 hours, respectively, during the fiscal year 2008. Fig.1 shows the accelerator operation hours per month. Fig.2 shows the beam time histogram with respect to the terminal voltage. Fig.3 represents the percentage of the operation hours for the three ion sources and ion species.

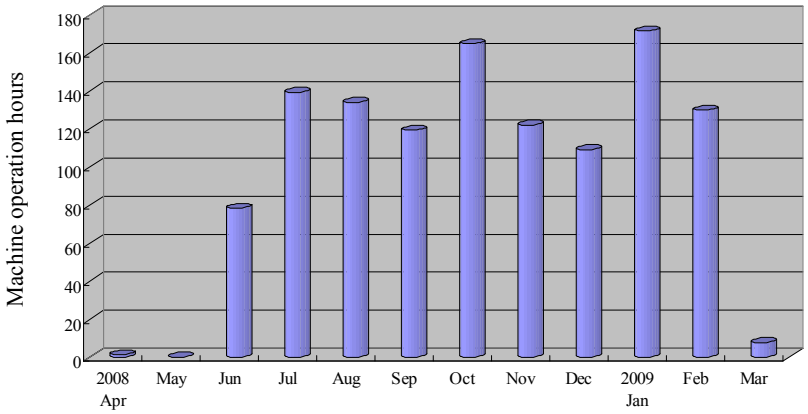

Fig.1. Accelerator operation hours per month for the 12UD Pelletron tandem accelerator in 2008.

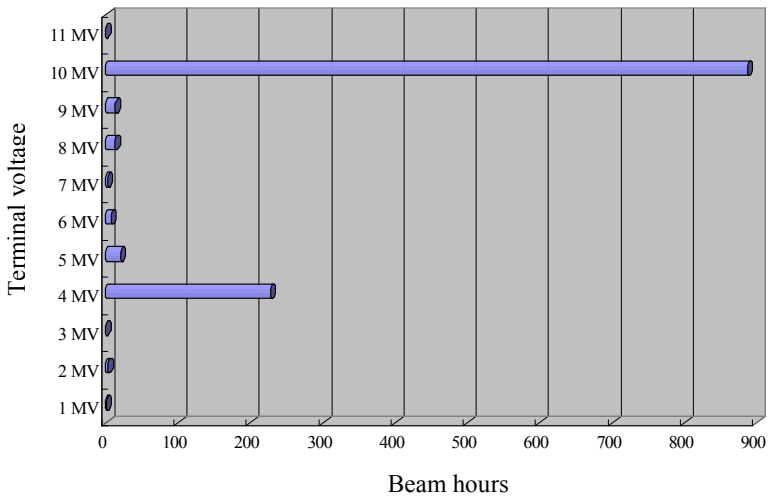

Fig.2. Beam time histogram as a function of the terminal voltage for the 12UD Pelletron tandem accelerator in 2008.

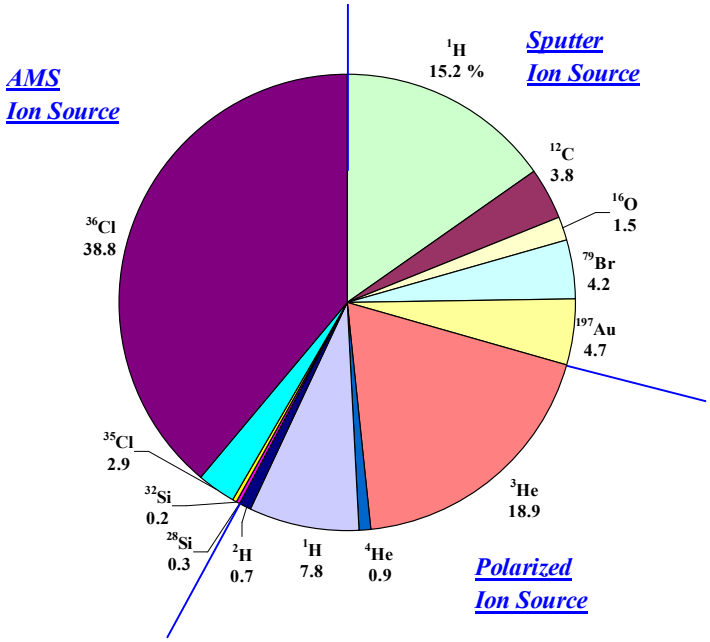

Fig.3. Percentage of the operation hours for the three ion sources and ion species in 2008.

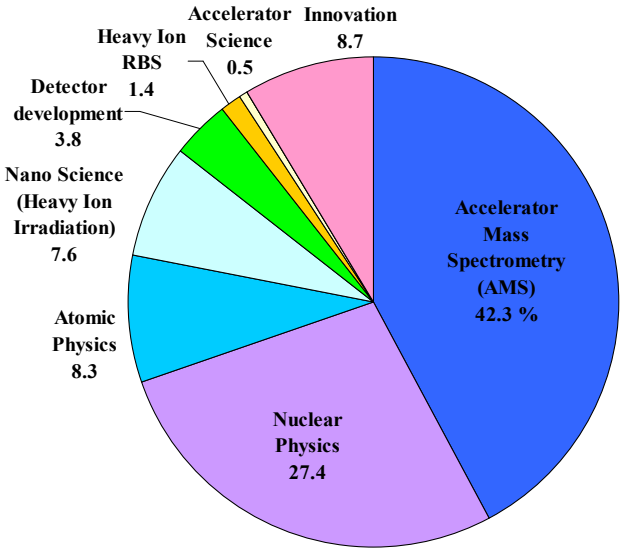

Fig.4. Percentage of the experimental beam time for the running research fields in 2008.

In 2008, 56 research programs were carried out using the 12UD Pelletron tandem accelerator. Totally, 556 researchers used the 12UD Pelletron tandem accelerator. Fig.4 shows the percentage of the experimental beam time for the running research fields with the 12UD Pelletron tandem accelerator.

The scheduled maintenance in the spring of 2009 was started on March 4. We replaced old corona needles with a divided resistor system during this period. Fig. 5 shows a photograph of the divided resister at the first unit. We adjusted the voltage gradient at the first unit in order to focus the ion beams on the terminal stripper position. At the first unit, a first accelerating tube was set to one third gradient. On the other hand, a 2nd accelerating tube was set to half gradient. The divided resister system allows the terminal voltage to vary from 1 to 11 MV without shorting column units. The divided resister system is

also expected to improve the stability of the terminal voltage. Fig. 6 shows the relationships between the charging current and the terminal voltage for corona needles and the divided resistor system. There are appreciable differences in the gradient of the terminal voltage generation. In the case of the divided resister system, the terminal voltage is proportional to the charging current.

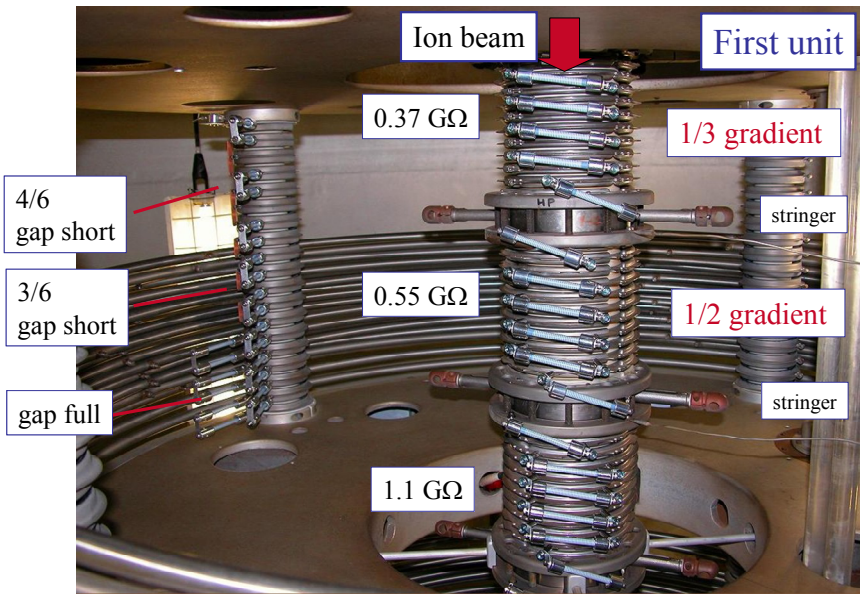

Fig.5. A photograph of the divided resister system at the first unit of the 12UD Pelletron tandem accelerator.

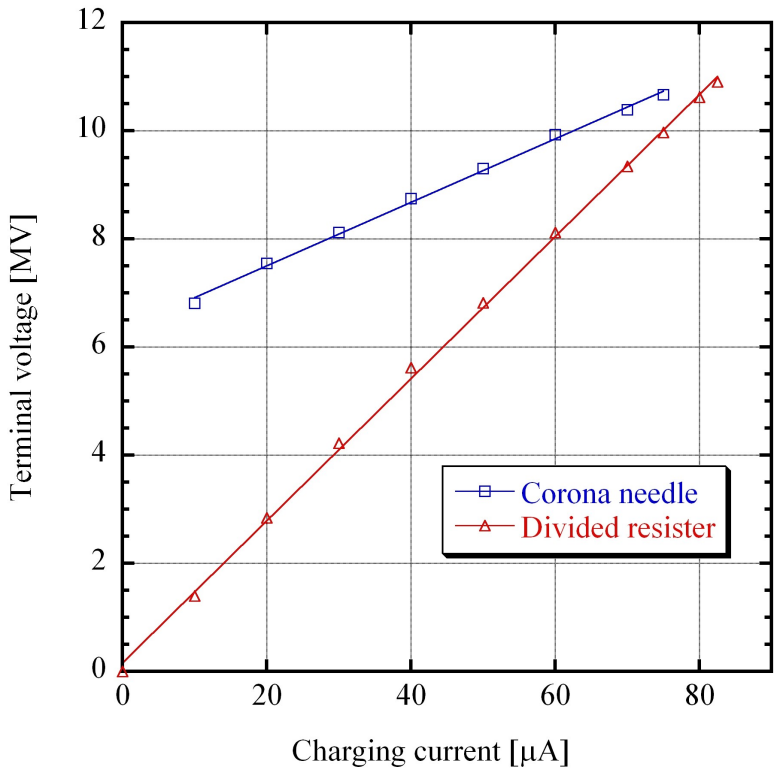

Fig. 6. The relationships between the charging current and the terminal voltage for corona needles and the divided resistor system.

Fig. 7 shows the proton beam transmission for various terminal voltages without shorting column units. The beam transmissions were measured between the object point on the injection magnet (FC-2) and the analyzer magnet (FC-5), under the condition of the injected proton current of 100 nA. The SF_6 gas recovery system was also repaired during the scheduled maintenance. We replaced a vacuum pumping system for SF_6 gas.

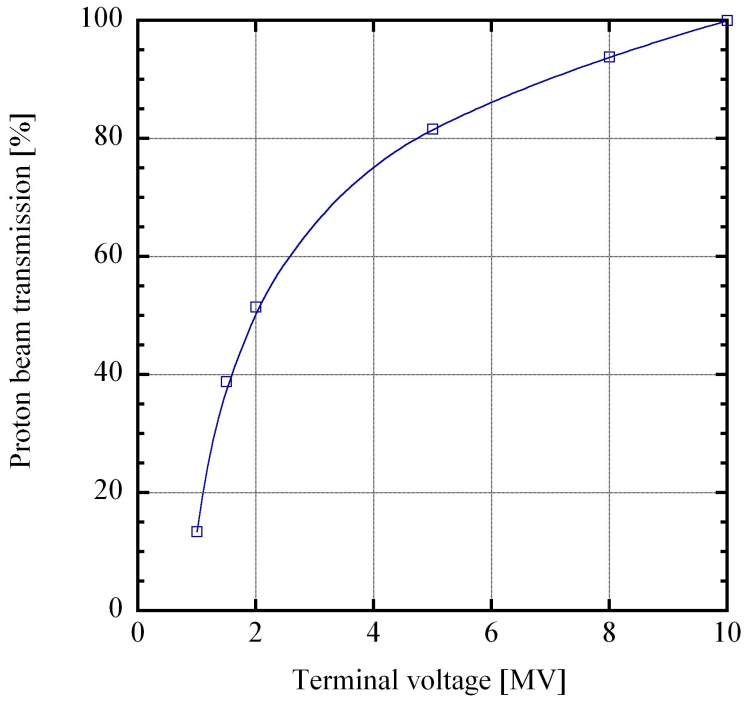

Fig.7. Proton beam transmission for various terminal voltages without shorting column units.

The 1MV Tandetron accelerator

The operating time and the experimental beam time of the 1MV Tandetron accelerator were 485.2 and 273.0 hours, respectively, during the total service time. In 2008, 41 research programs were carried out using the 1 MV Tandetron accelerator. Totally, 216 researchers used the 1MV Tandetron accelerator. Fig. 8 shows the percentage of accelerated ions for the 1MV Tandetron accelerator. Fig. 9 shows the percentage of the experimental beam time for the running research fields. The 1MV Tandetron accelerator was mainly used for trace-element analysis with Particle Induced X-ray Emission (PIXE), Rutherford Backscattering Spectroscopy (RBS), Elastic Recoil Detection Analysis (ERDA) and Cluster physics. In 2008, a new RBS/ERDA system was installed in the C beam line (15°-course).

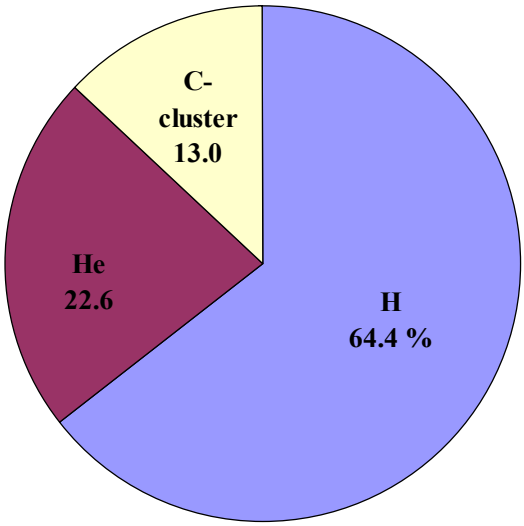

Fig.8. Percentage of accelerated ions for the 1 MV Tandetron accelerator in 2008.

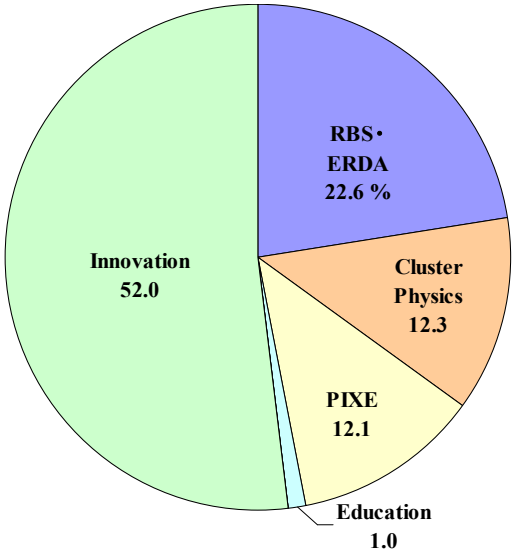

Fig.9. Percentage of the experimental beam time for the running research fields with the 1 MV Tandetron accelerator in 2008.

1.2 Status of the Tsukuba AMS system (2008)

K. Sasa, T. Takahashi, Y. Tosaki, K. Sueki, M. Tamari, T. Amano, T. Oki, Y. Yamato, Y. Nagashima, K. Bessho[1], H. Matsumura[1], N. Kinoshita[1] and Y. Matsushi[2]

We present the current status and research programs of a multinuclide accelerator mass spectrometry (AMS) system on the 12UD Pelletron tandem accelerator at the University of Tsukuba (Tsukuba AMS system) in 2008. The Tsukuba AMS system can measure environmental levels of long-lived radioisotopes of ^{14}C, ^{26}Al, ^{36}Cl and ^{129}I by employing a molecular pilot beam. We measured 365 samples in 2008, including samples for earth and environmental sciences and nuclear safety research. Total operation of AMS facility was 56 days in 2008.

Table 1 Research programs and the number of samples by the Tsukuba AMS system in 2008.

AMS research programs	Target material	Organization	Number
^{36}Cl-AMS			
^{36}Cl in the Dome Fuji ice core, Antarctica	Antarctic ice core	Univ. of Tsukuba	76
^{36}Cl in the radiation shield at accelerator facilities	Concrete	KEK	15
Bomb-produced ^{36}Cl as a tracer in groundwater	Hydrological samples (ground water, rain water)	Univ. of Tsukuba	83
In-situ ^{36}Cl for denudation rates of karst landform	Limestone	The Univ. of Tokyo	51
^{36}Cl in meteorite	Meteorite	Tokyo Metro. Univ.	25
Development of the chemical procedure for sulfur reduction	Environmental samples (soil)	Univ. of Tsukuba	91
Environmental monitoring for nuclear facilities by AMS	Environmental samples	Univ. of Tsukuba	9
^{36}Cl interlaboratory comparisons	Standard samples	Univ. of Tsukuba	11
^{36}Cl exposure dating for Tiankeng limestone samples	Limestone	CIAE, Guangxi University	2
^{32}Si-AMS			
^{32}Si-AMS research and development	SiO_2	Univ. of Tsukuba	2

Performance of the Tsukuba AMS system

The performance of ^{36}Cl-AMS was enhanced by improving the AMS technique and system, including modifying the sample preparation technique [1], upgrading the ion source and installing a new data acquisition system. Beam currents of $^{35}Cl^-$ and $^{37}Cl^-$ could be measured by the offset Faraday cups with the beam-current monitoring system [2]. A typical beam current for $^{35}Cl^-$ was up to 20 μA. $^{36}Cl^{14+}$

[1] Radiation Science Center, High Energy Accelerator Research Organization
[2] Micro Analysis Laboratory, Tandem Accelerator, The University of Tokyo

with an energy of 100 MeV is detected by the gas ΔE – SSD E detector. The standard deviation of fluctuations is typically ± 2%, and the machine background level for the ^{36}Cl/Cl ratio is lower than 1 × 10^{-15} with a halite sample, as shown in Figure 1(b) [2]. The AMS system achieved complete discrimination between ^{36}Cl and ^{36}S up to a counting rate of ~5 kHz.

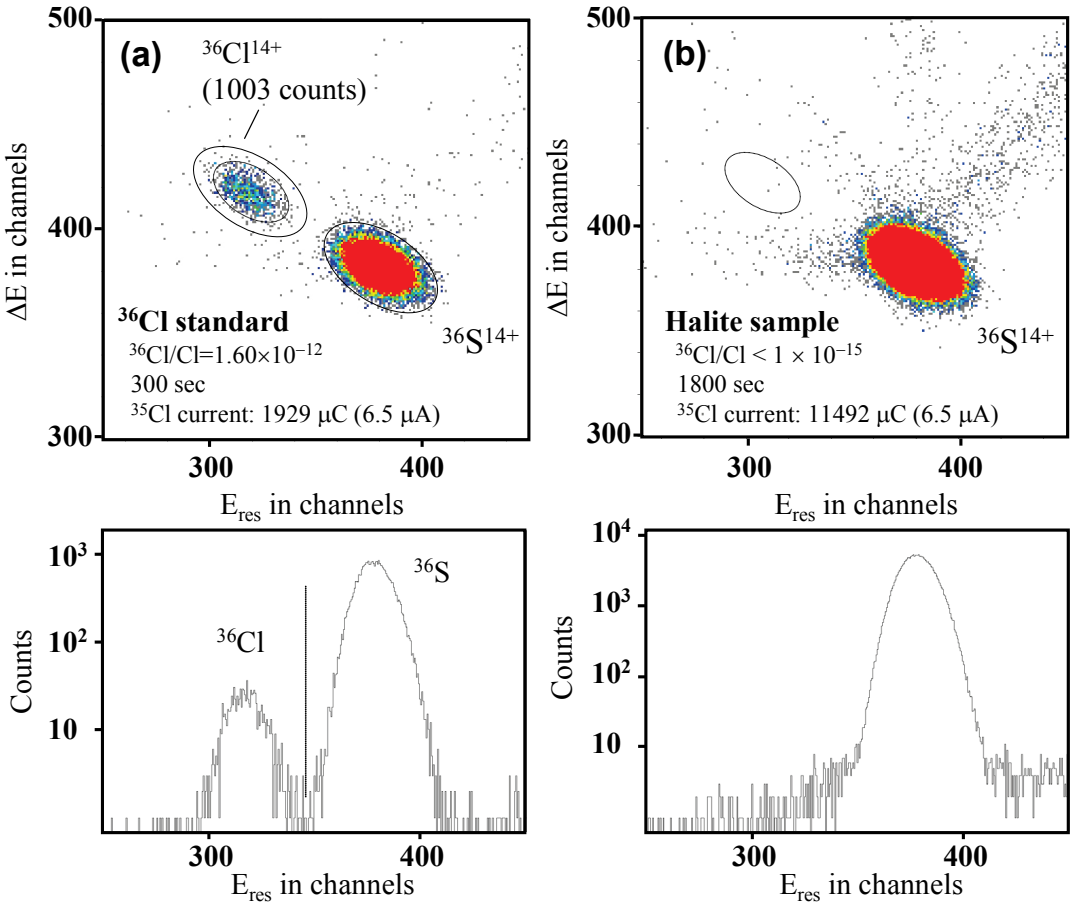

Fig. 1 (a) ^{36}Cl spectrum of a standard sample for ^{36}Cl/Cl = 1.60 × 10^{-12}. (b) ^{36}Cl spectrum of a halite sample for the system background check. Total of three counts of ^{36}Cl are detected for 30-min measurement. The background level is less than ^{36}Cl/Cl = 1 × 10^{-15}.

Acknowledgements

This work was supported in part by Grants-in-Aid for Scientific Research Programs of the Ministry of Education, Culture, Sports, Science and Technology, Japan (Grant-in-Aid Nos. 18360043, 19201003, 19300304, and 21310004) and the Promotion of Collaborative Research Programs in Universities, KEK.

References

[1] Y. Tosaki et al., Nucl. Instr. and Meth. B 259 (2007) 479.

[2] K. Sasa et al., Nucl. Instrum. Methods Phys. Res. B, 2009, in press.

1.3 Development of tilted electrode gas ionization chamber with high-rate

K.Ogawa, A.Ozawa, Y.Yasuda, K.Hara, T.Moriguchi, Y.Ito, H.Ooishi, Y.Ishibashi

We have been developing tilted electrode gas ionization chambers (TEGIC) as energy-loss detectors for RI beams. Detection of energy-loss is indispensable for particle identification. It is known that energy resolution of the detectors becomes worse at high counting-rate. Thus, we develop TEGIC, which can be used at the high counting-rate (~10^6 cps). A cross-sectional view of TEGIC is shown in Fig.1, where its electrodes are tilted by 60° from the beam axis. In the previous experiment, rate dependences of energy resolution have been measured with two different gases; P-10 and Ar-CF_4 [1]. In this measurement, energy resolution with P-10 becomes worse in the high-rate (~10^6 cps), on the other hand, energy resolution with Ar-CF_4 is almost constant for the counting rate. Recently, tilted-angle dependences of energy resolution were investigated. The results show that there was no difference in the energy resolution between 60° and 90° tilted-angles with the 10^3 cps counting-rate [2]. Thus, in the present experiment, we investigate the tilted-angle dependences of energy resolution in the high-rate and try to confirm the difference of the energy resolution with two gases.

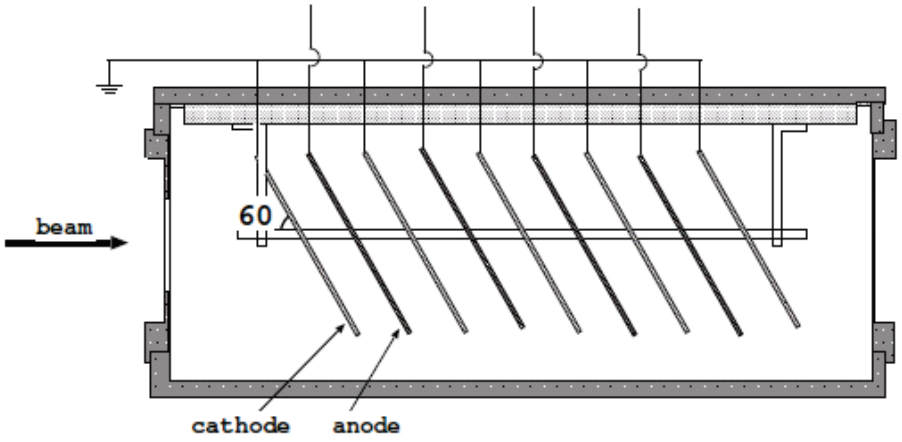

Fig.1 A cross-sectional view of TEGIC.

The experiment was carried out at the 12UD Pelletron tandem accelerator. Ion beam of ^{12}C nucleus was accelerated up to 60MeV. The ^{12}C beam, which was scattered elastically by a gold 2μm target to adjust the beam intensity, was irradiated to TEGIC. The beam intensity was increased to 10^6 cps. TEGIC was operated using P-10 and Ar-CF_4 with about 130 Torr. Counting-rate dependences of the energy resolution with different tilted-angles are shown in Fig.2. In the high counting-rate (more than 10^5 cps), energy resolution becomes worse in two different tilted-angles. Counting-rate dependences of the energy resolution with different gases are shown in Fig. 3. Here, the energy resolutions in the two gases become worse in the high counting-rate similarly. The present results are not consistent with the previous ones. Further analysis is in progress.

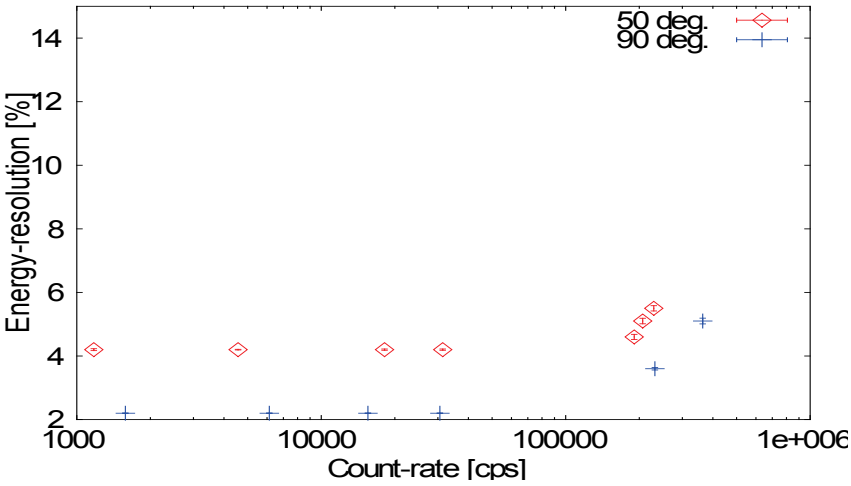

Fig.2 Counting-rate dependences of the energy resolution with two different tilted-angles (50 deg. and 90 deg.). The diamond shape is 50 deg. Line is 90 deg.

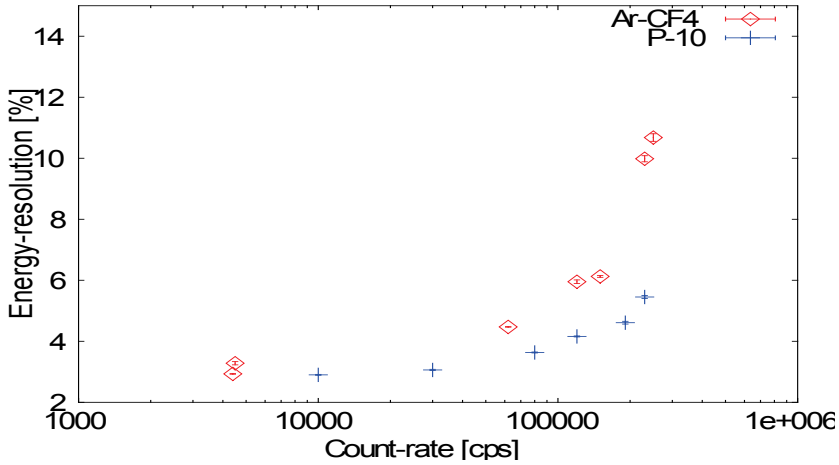

Fig.3 Counting-rate dependences of the energy resolution with two different gases (P-10 and Ar-CF_4). The diamond shape is Ar-CF_4 gas. Line is P-10 gas.

References

[1] K.Kimura, et.,al., Nuclear Instromental & Methods in Physical Resarch A 538(2005)608-614.

[2] Y.Yasuno, University of Tsukuba, Master thesis (2006).

2.

NUCLEAR PHYSICS

2.1 Measurement of nuclear magnetic moment of unstable nucleus ^{40}Sc

Y.Ishibashi, A.Ozawa, Y.Tagishi, M.Iijima, Y.Ito, H.Ooishi, K.Ogawa, T.Moriguchi, Y.Yasuda, T.Nagatomo[1] and K.Matsuta[2]

The unstable nucleus ^{40}Sc (half life $T_{1/2}$=182 ms) is located near stable nucleus ^{40}Ca, which is a doubly closed shell nucleus. Thus, its nuclear structure is interesting. However, the nuclear magnetic moment (μ) of ^{40}Sc has never been measured. Since μ is sensitive to the configuration mixing in the nucleus, we started to measure ^{40}Sc.

Polarized ^{40}Sc nucleus was produced at UTTAC by using ^{40}Ca($\vec{p}$,n)^{40}Sc (Q=-15.105 MeV) reaction. A 20 MeV polarized proton beam (P=88%) from the tandem accelerator irradiated a CaF_2 crystal target with a thickness of 3 mm. The intensity of polarized proton beam was ~3 nA. Fig.1 shows setup around the target. The polarized proton beam was transported to the beam line of F-course in the first experimental room and was stopped in CaF_2 crystal. Primary beam was chopped by a beam chopper., which was located at the entrance of the F-course. The beam chopper is a rotatable Cu cylinder with windows, as shown in Fig. 2, and controls the primary beam with on : off=1:2.

To measure μ of ^{40}Sc, we applied the β-NMR method [1]. The experimental setup for β-NMR is shown in Fig.1. To keep nuclear polarization of ^{40}Sc inside the stopper, a static magnetic field (~2.5 kG) was applied. A Helmholtz-type coil surrounded by the stopper produced a radio-frequency (RF) magnetic field (~1.8 MHz, ~5 G) to perform NMR. The detectors located in up and down of the stopper counted the number of β-rays emitted from the stopped ^{40}Sc. To search for the μ of ^{40}Sc, we measured up and down ratio of β-rays while changing the frequency of RF.

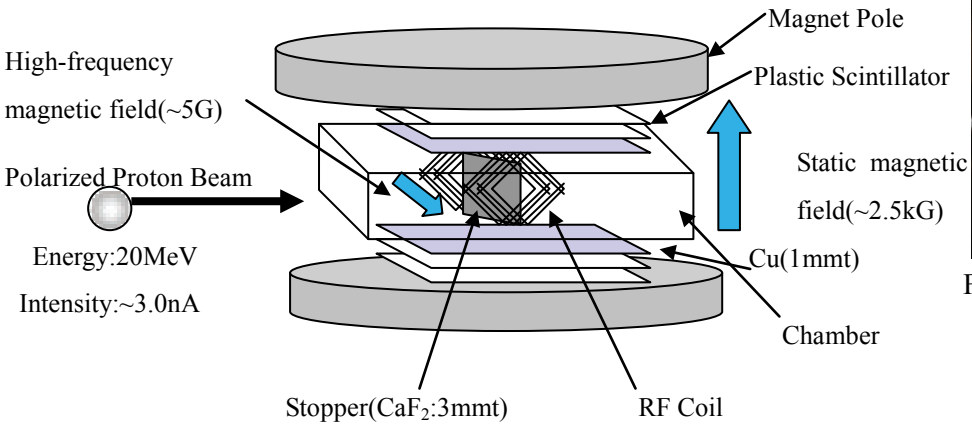

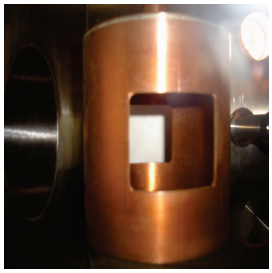

Fig.2. Beam chopper.

Fig.1. Experimental setup around the target. Two plastic scintillators were used to detect β-rays. Cu absorber located between the detectors and the chamber to cutlow energy β-rays.

We observed β-rays for 600 ms after the beam was stopped. Fig.3 (a) shows an observed typical time spectrum of the β-rays.

[1] RIKEN, Wako, Saitama 351-0198, Japan
[2] Department of Physics, Osaka University, Toyonaka, Osaka 560-0043, Japan

In Fig.3 (a), typical time spectrum for the β-rays is shown. Here, component of ^{40}Sc is clearly seen in the first 120 ms. However, background is dominant in the last 120 ms. Observed NMR spectra for ^{40}Sc is shown in Fig. 3 (b), where we extracted asymmetry changes observed in the last 120 ms from those in the first 120 ms. We measured NMR spectra with three different RF widths (160 kHz, 300 kHz, and 500 kHz). To search for the magnetic moment, we averaged results with the different RF widths in the corresponding magnetic moment in Fig. 3 (b), thus, the spectrum shown in Fig.3 (c) was obtained. We may see some asymmetry change near the $|\mu|$=5.1 μ_N. To confirm this, further investigation is needed. Observed nuclear polarization is very small in the present measurements, so it is necessary to increase asymmetry change. We will apply higher static magnetic field and decrease background of β-rays in the future measurements.

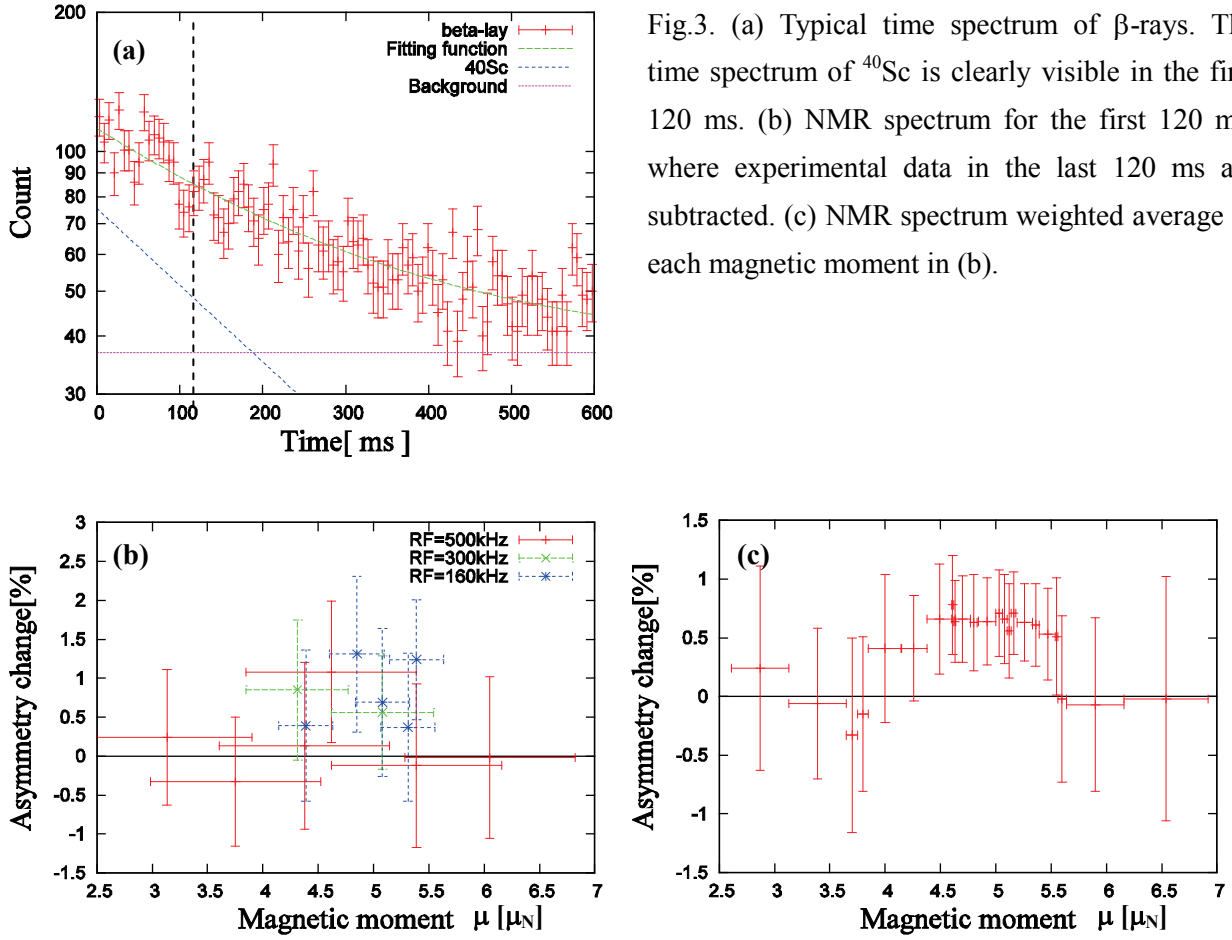

Fig.3. (a) Typical time spectrum of β-rays. The time spectrum of ^{40}Sc is clearly visible in the first 120 ms. (b) NMR spectrum for the first 120 ms. where experimental data in the last 120 ms are subtracted. (c) NMR spectrum weighted average of each magnetic moment in (b).

References

[1] C.P. Slichter , Principles of magnetic resonance, 3rd enlarged and updated ed.

2.2 Study of nuclear synthesis of ^{26}Al by gamma ray spectroscopy II

T. Komatsubara, A. Ozawa, K. Hara, T. Moriguchi, Y. Ito, H. Satake, H. Ooishi, Y. Ishibashi, T. Shizuma*, T. Hayakawa*, S. Kubono[#], S. Hayakawa[#], D.N. Binh[#], D. Kahl[#], A. Chen[%] and J. Chen[%]

* JAEA

[#] CNS, Tokyo University

[%]McMaster University, CANADA

Since observation of 1.809-MeV gamma rays by satellite gamma ray telescope has been reported[1], the astrophysical study of ^{26}Al is very important for nuclear synthesis. The nucleus ^{26}Al can be created by ^{25}Mg(p,γ) reaction. However there is bypass reaction sequence ^{25}Al(p,γ)^{26}Si(β,ν)^{26m}Al(β,ν) which emits no gamma ray of 1.809 MeV. The excited states of ^{26}Si, key nucleus, have been studied by reaction mechanism[2-5] and gamma ray spectroscopy[6]. In our previous study, one new level is found above proton threshold at 5886-keV in the ^{26}Si[7]. For the determination of spin of the observed state, gamma-ray angular correlation measurements were carried out.

In order to investigate level structure in ^{26}Si, in-beam gamma ray spectroscopy was performed at UTTAC. The excited states of the ^{26}Si were populated by the nuclear reaction ^{24}Mg(^{3}He,n)^{26}Si. The ^{3}He beam of 10 MeV was irradiated on a natural Mg target. Gamma-gamma coincidence measurements were performed by using Ge detectors. Relative efficiencies of the Ge detectors are 140% and 70% at 1333-keV.

For the determination of spins, ratios of directional angular correlation of gamma-rays from oriented states (DCO ratios)[8] have been evaluated. The larger Ge detector was located at 135 degree with respect to the beam axis, while other was at 90 degree. For the values of 90-90 degree correlation, gamma-gamma coincidence data taken in the last year were re-analyzed.

As the results of the DCO measurement, the ratios are shown as closed circles in Fig. 1 as a function of the gamma ray energy. The gate gamma ray is 1797-keV $2^+ \rightarrow 0^+$ transition. In this figure, theoretical expectation values are also shown as open triangles. In this calculation initial distribution of magnetic sub-state is assumed by following distribution;

$$P(m) = \frac{e^{-\frac{m^2}{2\sigma^2}}}{\sum_{x=-J}^{J} e^{-\frac{x^2}{2\sigma^2}}}.$$

where the σ is assumed to be 2.0 J. Mixing ratios are also assumed to be zero.

For the gamma rays of 989- and 1960-keV transitions, measured values of DCO ratio agree with the calculation within the errors where those are 2→2→0 and 3→2→0 transitions, respectively. For the 1537-keV, small value of the DCO ratio is rather consistent with the calculation of 0→2→0 transition.

References

[1] R. Diehl, H. Halloin, K. Kretschmer, G.G. Lichti, V. Schönfelder, A.W. Strong, A. Kienlin, W. Wang, P. Jean, J. Knödlseder, J.P. Roques, G. Weidenspointner, S. Schanne, D.H. Hartmann, C. Winkler, C. Wunderer, Nature 439 (2006) 45.

[2] D.W. Bardayan, J.C. Blackmon, A.E. Champagne, A.K. Dummer, T. Davinson, U. Greife, D. Hill, C. Iliadis, B.A. Johnson, R.L. Kozub, C.S. Lee, M.S. Smith, P.J. Woods, Phys. Rev. C 65 (2002) 032801(R).

[3] J.A. Caggiano, W.B. Smith, R. Lewis, P.D. Parker, D.W. Visser, J.P. Greene, K.E. Rehm, D.W. Bardayan, A.E. Champagne, Phys. Rev. C 65 (2002) 055801.

[4] Y. Parpottas, S. M. Grimes, S. Al-Quraishi, C.R. Brune, T.N. Massey, J.E. Oldendick, A. Salas, T. Wheeler, Phys. Rev. C 70 (2004) 065805.

[5] P.N. Replowski, L.T. Baby, I. Wiedenhöver, S.E. Dekat, E. Diffenderfer, D.L. Gay, O. Grubor-Urosevic, P. Höflich, R.A. Kaye, N. Keeley, A. Rojas, A. Volya, Phys. Rev. C 79 (2009) 032801(R).

[6] D. Seweryniak, P.J. Woods, M.P. Carpenter, T. Davinson, R.V.F. Janssens, D.G. Jenkins, T. Lauritsen, C.J. Lister, J. Shergur, S. Sinha, A. Woehr, Phys. Rev. C 75 (2007) 062801(R).

[7] T. Komatsubara, K. Ebisu, T. Kawamata, A. Ozawa, K. Hara, T. Moriguchi, Y. Hashizume, T. Shizuma, T. Hayakawa, S. Kubono, UTTAC Annual Report 2007, UTTAC-77 (2008) pp15-16.

[8] K.S. Krane, R.M. Steffen, R.M. Wheeler, Nuclear Data Tables, 11, (1973) 351.

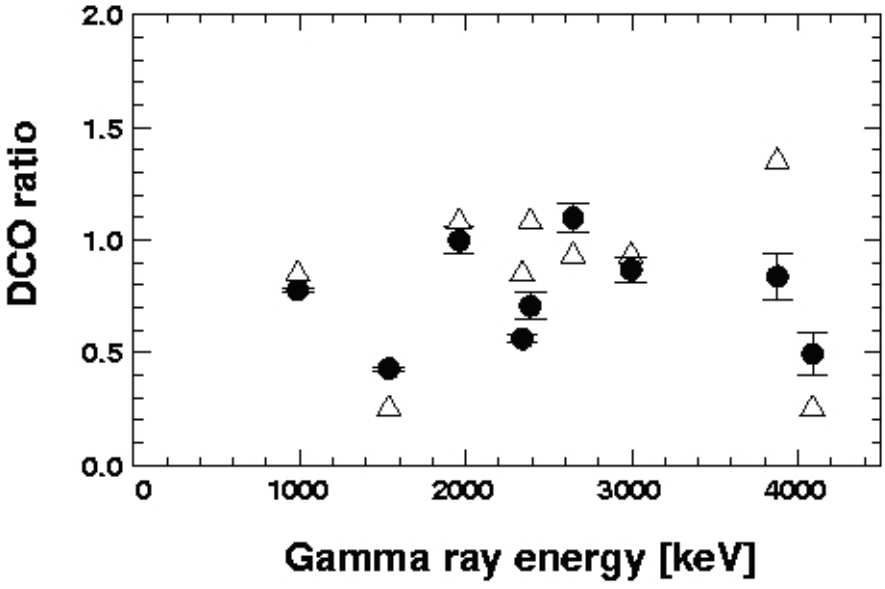

Fig.1 DCO ratios for ^{26}Si.

3.

MATERIALS AND CLUSTER SCIENCE

3.1 RBS study on Mg_4NiH_x system

D. Sekiba, S. Abe, M. Horikoshi, H. Kudo

Mg_2Ni has been studied by many techniques because this alloy shows good absorption ability for hydrogen. Hydrogen storing alloys are important from the viewpoint of the sustainable energy. On the other hand, many hydrogen storing alloys, which consist of Mg, show a remarkable property that metal-insulator transition due to the hydrogenation. This transition is reversible for the hydrogenation and dehydrogenation. Mg_2Ni and Mg_2NiH_4 are reflective and transparent for the visible light, so that this material is called switchable mirror. Apart from the Mg_2Ni, other Mg-based alloys such as Mg-Co, Mg-Ti, Mg-Fe show a similar phenomenon.

A problem to be solved for the practical use of the Mg-Ni switchable mirror is the poor switching durability. To elucidate the mechanism of degradation of the device, we constructed a new small chamber in which the Mg-Ni thin film is hydrogenated and dehydrogenated automatically by computer-controlled gas inlet system. The samples were prepared by DC magnetron sputtering. We made Mg_4Ni, referring the report by Yoshimura et al. [1], on Si and glass substrate with the film thickness of 40 nm and 5 nm thick Pd cap layer. We made a comparative study of RBS (Rutherford back scattering) on the both as-deposited and retrograded sample by 120 times switching. 1.6 MeV ^4He was used as an incident beam, and the scattered ions were collected at the angle of 150 degree with respect to the incident direction.

Figure 1 shows RBS spectra obtained. The three peak features at ~ 0.6 MeV, ~ 0.8 MeV and ~ 1.2 MeV are attributed to oxygen, Mg and Ni, respectively. We can see that the Ni peak shifts toward the lower energy, while the leading edges of Mg peaks are coincident between the as-deposited and retrograded samples. The O peak is observed only on the retrograded sample. By the analysis of these data we found out that Mg_4Ni showed a phase separation to the stoicheiometric Mg_2Ni and Mg layers. The segregated Mg layer below the Pd cap layer might construct stable hydride and oxide and play a role of blocking layer for the hydrogen permeation.

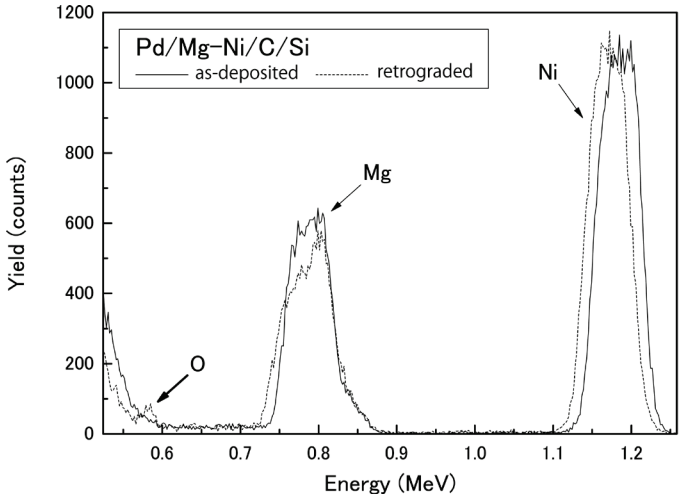

Fig. 1: RBS spectra taken on the as-deposited and retrograded samples. 1.6 MeV $^4He^{2+}$ ion was used as an incident beam and scattered ions were collected at the angle of 150 degree with respect to the beam incident direction.

References

[1] K. Yoshimura, Y. Yamada, M. Okada, Appl. Phys. Lett. 81 (2002) 4709.

3.2 Temperature dependence of hyperfine fields in spinel type Fe_3O_4 nano-particles

M. Minagawa, H. Yanagihara, E. Kita and M. Kishimoto[1]

Magnetic hyperthermia has been a new therapy for small and spread cancerous tumors, because it dose not need surgical operations. Using nano-sized magnetic particles and selective adhesion based on the antigen-antibody reaction between the particles and cancer tumors, effective application of heat power on the particular cells can be achieved. Particles are necessary to move in the human bodies, then sizes of the magnetic particles are limited to be small less than several tens of nano-meters. A few mechanisms of heating with magnetic fine particles are considered, such as relaxation heating in superparamagnetic(SPM) states (Neel mechanism), ferromagnetic hysteresis loss heating and frictional motion of magnetic particles.[1] Most of researches are using SPM particles in which particle aggregation of particles is small. Very large specific loss power (SLP) has been expected in the narrow distribution of particle sizes and, in other words, there are severe conditions in size and distribution of magnetic nanoparticles and driving frequency. If ferromagnetic nanoparticles can be used for hyperthermia, there is much less limitation for tuning of operation conditions.

We have been testing the ability of ferromagnetic nano-particles with rather higher coercive force as a hyperthermia material[2]. To understand the relation between coercive force and heating ability, magnetic states of nano particles are an important issue. We performed Mössbauer study to understand the influence of thermal fluctuation on the ferromagnetic state of nano-particles.

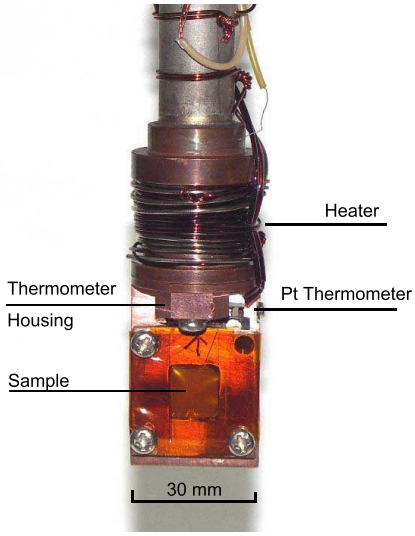

Fig. 1. Sample holder part of Mössbauer measurement oven. Temperature range from room temperature to 200°C can be achieved. The heater is made of a type E fine sheath thermocouple. A Pt resistance thermometer is set into the housing.

Cobalt-contained iron oxide particles with spinel structure, $(Co)Fe_{3-\delta}O_4$, were produced by heating the co-precipitants containing Co^{2+}, Fe^{2+} and Fe^{3+} ions.[2] Spinel structures were confirmed with X-

[1]Hitachi Maxell, Ltd.

ray diffraction patterns. The coercive forces (H_C) from 50 Oe to 240 Oe were obtained by changing the content of Co ions from 2 $\sim$ 7 at% of total Fe ions. Sizes of nano-particles were ranged between 10 and 20 nm. Sample ATH1 (pure Fe oxide with H_C of 50 Oe) and ATH4 (Co doped Fe oxide with H_C of 160 Oe) were used for Mössbauer measurements. To perform high temperature measurements between room temperature and 200°C, a new sample oven was built(see Fig. 1). The sample temperature was measured with a Pt thermometer. Data were analyzed with a commercially available software, MossWinn 3.0. Distribution in hyperfine field(H_{hf}) was taken into account carried out in the analysis.

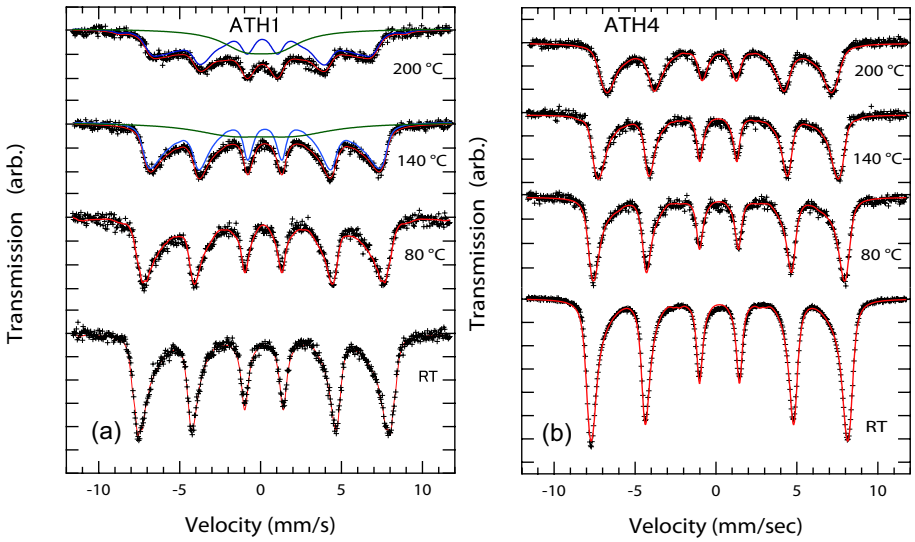

Fig. 2. Mössbauer spectrum of the samples ATH1 and ATH4 at the temperature range between room temperature and 200 °C. Solid lines display results of numerical fitting.

Mössbauer spectra for ATH1 and ATH4 samples are show in Figs. 2 (a) and (b), respectively. At room temperature, ferromagnetic sextets with slightly spread hyperfine fields were observed in both samples and no trace of SPM contribution was found. Elevating sample temperature, the spectra for the ATH1 above 140 °C composed of a major ferromagnetic sextet and a doublet which is originated from an SPM state. This result suggests that ATH1 has two magnetic phase above 140 °C and the ferromagnetic state in ATH1 is relatively weak. ON the other hand, feromagnetism in the ATH4 sample is stable even at 200 °C. Higher heat generation has been proved by applying AC high magnetic field test for ATH4 samples than the ATH1 sample.

This work is a part of a cooperative research carrying out with digestive surgery group in University of Tsukuba and AIST.

References

[1] for example, see R. Hergt and W. Andrä, *Magnetism in Medicine* Wiley-VCH, Weinheim 2007, p. 550.

[2] Eiji Kita, H. Yanagihara, S. Hashimoto, K. Yamada, T. Oda, M. Kishimoto, and A. Tasaki, IEEE Trans Magn., vol. 42 pp. 3566-3568, 2008.

3.3 Fabrication of aligned pairs of gold nanowires in SiO_2 films by ion irradiation

Koichi Awazu, [1] Xiaomin Wang,[1] Tetsuro Komatsubara

Introduction

It has been found that anisotropic metal colloids can be fabricated in a controllable manner by irradiation of core-shell colloidal particles by swift ions of megaelectron volt (MeV) energy, where each colloidal particle has a Au core surrounded by a silica shell. [1] However, it has been pointed out that the process of Au elongation could be very complicated. For example, the uncontrolled nucleation and growth processes results in broad spatial and size distribution of the nanoparticles during ion irradiation.[2] Heinig and coworkers [3] reported that the mean size of Au nanoparticles in SiO_2 theoretically increases with increasing implantation temperature, a process known as Ostwald ripening, but that inverse Ostwald ripening occurs below a certain critical temperature. To avoid these kinds of complicated matters, we used electron-beam lithography to fabricate Au nanoparticles of a constant diameter spaced a constant relatively large distance apart in a SiO_2 matrix, and we examined the dependence of the elongation of the nanoparticles on their initial size and on the fluence and flux of the ion beam.

Experimental procedure

To form the substrate, a 2-μm-thick layer of amorphous SiO_2 (a-SiO_2) was fabricated by surface oxidation of a silicon wafer with water vapor at 1000 °C. The a-SiO_2 substrate was spin-coated with a 50-nm-thick layer of ZEP520-type resist, and the coating layer was cured at 180 °C for 3 min. Nanoscale patterns were drawn in a 200 × 200 μm region of the resist by electron-beam lithography. Subsequent development produced pairs of nanoscale holes in the resist on the a-SiO_2 substrate. The substrate was then mounted in an evaporator and a 0.5-nm-thickCr layer was applied to aid adhesion of a subsequently deposited 40-nm-thick layer of Au. Next, the resist was removed by treatment with acetone to leave an array of pairs of Au nanodisks on the a-SiO_2 substrate. The Au nanodisk pairs were then embedded in a-SiO_2 by depositing a second layer of silica by sputtering from a silica target in an Ar atmosphere. The thickness of the top layer of a-SiO_2 was 200 nm. The final assemblies were irradiated with 110-MeV Br^{10+} ions produced by the 12-unit double Pelletron tandem accelerator at University of Tsukuba. The beam current was changed from 10 nA to 60 nA to examine the effect of the flux density. Flux density was calculated from the beam current, where a beam current of 100 nA corresponded to $(2.8 \pm 0.3) \times 10^{11}$ cm^{-2} s^{-1}. The direction of propagation of the ion beam was perpendicular to the upper surface of the a-SiO_2. Cross-sections of the pristine and irradiated samples were examined by transmission electric microscopy (TEM).

Results and Discussion

We examined the dependence of elongation of Au nanodisks on the flux density of the ion beam at a constant fluence. Figures (a)– (d) show Au nanoparticles embedded in SiO_2 before irradiation (Fig. (a))

and after irradiation with 110-MeV Br^{10+} ions at flux densities of 3×10^{10} cm^{-2} s^{-1} [Fig. (b)], 6×10^{10} cm^{-2} s^{-1} [Fig. (c)], and 1.6×10^{11} cm^{-2} s^{-1} [Fig. (d)] at a constant fluence of 2×10^{14} cm^{-2}. The aspect ratio of the nanorods increased markedly with increasing flux density up to a flux density of 6×10^{10} cm^{-2} s^{-1} in the direction of propagation of the ion beam. The aspect ratio reached 20 at a flux density of 6×10^{10} cm^{-2} s^{-1}. At a flux density of 1.6×10^{11} cm^{-2} s^{-1}, however, the positions, as well as the lengths, of Au nanodisks pairs were changed (Fig. (d)).

Summary

We successfully avoided Ostwald ripening by fabricating Au nanoparticles pairs with a constant separation of 60 nm. By this technique, the mechanism of elongation of Au nanoparticles was considerably simplified. Au nanodisks of diameter 40 nm were elongated in a manner dependent on flux density of ion irradiation. We assume that both the 40-nm-diameter Au nanoparticles and surrounding a-SiO_2 were melted during ion bombardment.

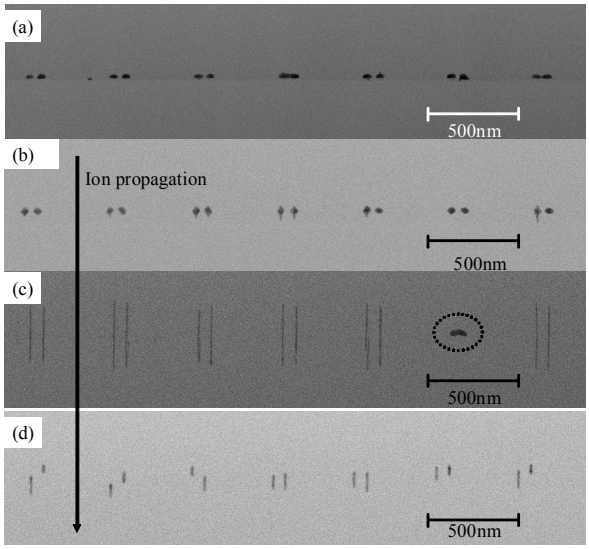

Figures. Bright-field and cross-sectional TEM micrographs. The flux density dependence of Au elongation was examined at a constant fluence of 2×10^{14} cm^{-2}. (a)–(c); Au nanodisks of 40 nm in diameter. Specimens were created with focused ion beam. (a); before irradiation of 110-MeV Br^{10+} ion. (b), (c), and (d); flux density of 3×10^{10} cm^{-2} s^{-1}, 6×10^{10} cm^{-2} s^{-1}, 1.6×10^{11} cm^{-2} s^{-1}, respectively. The direction of ion propagation direction is shown by the arrow.

References

[1] Roorda S, Dillen T V, Polman A, Graf C, Blaaderen A V and Kooi B J 2004 *Adv. Mater. 16* 235

[2] Rizza G,Ramjauny Y,Gasoin T, Vieille L and Henry S, 2007 Phys. Rev. B 76 245414

[3] Heinig K H, Müller T, Schmidt B, Strobel M and Möller W 2003 *Appl. Phys. A 77* 17

3.4 RBS of Pt and Cu nano-clusters on HOPG

T. Kondo, T. Suzuki, J. P. Oh, D. Sekiba, H. Kudo and J. Nakamura

Understanding the interface interaction between metal nano-clusters and the surfaces of graphite-related material is indispensable for many industrial applications such as catalysis. It has been found that Pt monolayer clusters, with a width of 2-3 nm, on a highly oriented pyrolytic graphite (HOPG) surface promote catalytic activity for the H_2-D_2 exchange reaction [1]. The origin of this enhancement has been attributed to the interface interaction between the Pt atoms and the graphite surface which leads to a shift in the d-band center of the Pt away from the Fermi level. This result suggests that even for the inert metal atoms for the H_2-D_2 exchange reaction such as Cu, the promoted catalytic activity may appear by forming monolayer cluster on the graphite surface through the interface interaction. In this work, we have investigated the catalytic activity of Cu/HOPG as well as Pt/HOPG in terms of H_2-D_2 exchange reaction.

Fig. 1a shows typical RBS spectra for HOPG, Pt/HOPG and Cu/HOPG. There is no peak originating from contaminants such as O_2 or other metal atoms, suggesting that the Pt or Cu atoms are successively deposited on HOPG without any contamination. Based on the spectra, the absolute amount of Pt or Cu on HOPG is estimated. The catalytic activities k_m of Pt/HOPG and Cu/HOPG for the H_2-D_2 exchange reaction measured in the high-pressure reactor-cell at 400 K under 24 Torr condition (H_2:D_2 = 1:1) are summarized in Fig. 1b as a function of the absolute coverage of Cu or Pt on HOPG.. The catalytic activity of Cu/HOPG is found to be 1-2 orders of magnitude smaller than that of Pt/HOPG. Similar low catalytic activity has also been reported for Cu films on HOPG [2]. Thus the Cu atoms deposited on HOPG in this work may form larger and thicker domains instead to form monolayer clusters with a width of 2-3 nm. By changing the deposition condition of Cu and measuring the morphology of Cu cluster by scanning tunneling microscopy, we will investigate the catalytic activity of Cu/HOPG more in detail.

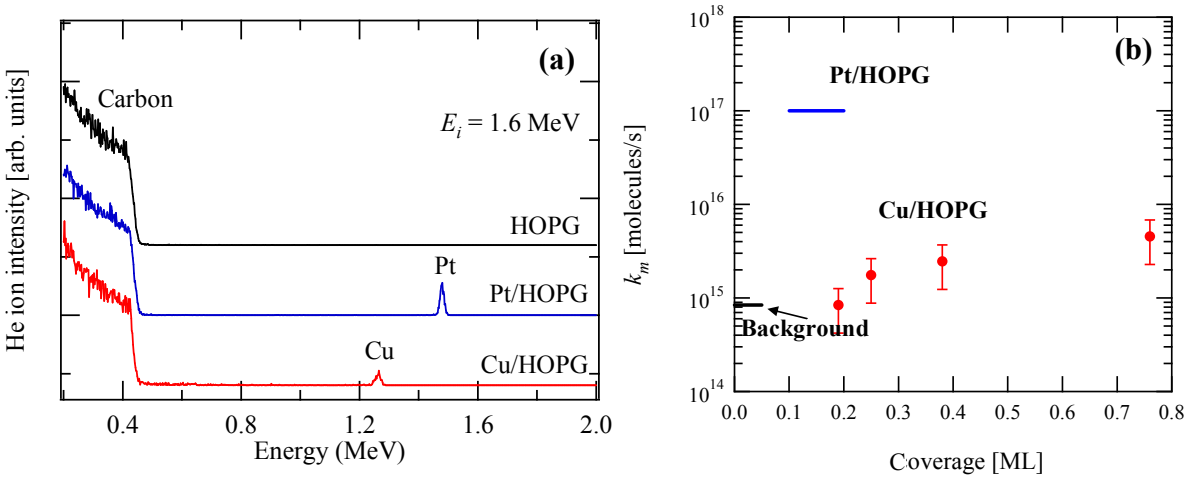

Fig. 1: (a) RBS spectra taken on the HOPG, Cu/HOPG and Pt/HOPG. 1.6 MeV $^4He^{2+}$ ion was used as an incident beam and scatted ions were collected at the angle of 150 degree with respect to the beam incident direction. (b) k_m of Cu/HOPG and Pt/HOPG for the H_2-D_2 exchange reaction.

References

[1] T. Kondo, K. Izumi, K. Watahiki, Y. Iwasaki, T. Suzuki, J. Nakamura, J. Phys. Chem. C **112** (2008) 15607.

[2] Johansson et al., J. Chem. Phys. **128** (2008) 034706.

4.

ACCELERATOR MASS SPECTROMETRY

4.1 Measurement of cosmogenic ^{36}Cl in the Dome Fuji ice core, Antarctica: Preliminary results for the Last Glacial Maximum and early Holocene

K. Sasa, Y. Matsushi[3], Y. Tosaki, M. Tamari, T. Takahashi, K. Sueki, T. Amano, T. Oki, Y. Nagashima, H. Matsumura[1], N. Kinoshita[1], K. Bessho[1], K. Horiuchi[2], H. Matsuzaki[3], Y. Shibata[4], M. Hirabayashi[5] and H. Motoyama[5]

We report the results of trial measurements of ^{36}Cl concentrations for ~150 g-size of ice per sample, with the aim of enabling routine analysis during planned high-resolution multi-nuclide research as part of the second deep-ice-core project at Dome Fuji Station (DF2) in Antarctica (77°19'01" S, 39°42'12" E; 3810 m above sea level) [1]. Samples analyzed were taken from those parts of the DF2 ice core corresponding to the Last Glacial Maximum (LGM) and early Holocene. We also present preliminary calculations of the depositional flux of cosmogenic ^{36}Cl for these periods, as an initial result from inland Antarctica.

Ten samples, obtained as ice chips produced from core trimmings for measurements of electrical conductivity, were analyzed for ^{36}Cl concentrations. These samples were obtained from 540 m, 490 m, and 340–320 m below the surface of the ice sheet, corresponding to ages of 22, 18, and 11–10 kyr according to the DFO-2006 age scale, respectively [2]. Each sample comprised 0.5 m in core length (110–180 g in weight), corresponding to a temporal resolution of approximately 30–40 years. ^{36}Cl-AMS was successfully conducted with at least ~100 counts of total ^{36}Cl detection for the ice samples. The full-processing chemistry blank yielded 0.6×10^{-14} of ^{36}Cl/Cl. The ^{36}Cl/Cl values for the ice samples range from 2×10^{-14} to 16×10^{-14} after subtraction of the background observed in the chemistry blank. The original chlorine concentrations in the LGM samples range from 210 to 260 ppb, corresponding to less than 5% of the carrier amount. The overall uncertainty in the measurements was ~10% for the Holocene samples with a larger carrier amount, and up to ~6% for the LGM samples. The ^{36}Cl concentrations in the ice samples range from 6×10^3 to 8×10^3 atoms g^{-1} for the early Holocene, and from 14×10^3 to 17×10^3 atoms g^{-1} for the LGM. The differences in concentrations between the two periods reflect contrasting rates of snow accumulation during glacial and interglacial periods. The annual net amount of snow accumulation can be estimated empirically from the δ^{18}O value of ice [3], which is about−60‰ for the LGM and −54‰ for the early Holocene [4], corresponding to snow accumulation rates of ~1.8 and ~4.3 g cm^{-2} yr^{-1}, respectively [3]. These rates differ by a factor of ~2.4; accordingly, the contrasting ^{36}Cl concentrations between the LGM and early Holocene are well explained by the dilution of nuclide fallout by snow deposition. The apparent depositional fluxes of ^{36}Cl onto the ice sheet were calculated from the nuclide concentrations multiplied by the snow accumulation rates. The calculated ^{36}Cl fluxes are nearly

[1] Radiation Science Center, High Energy Accelerator Research Organization
[2] Hirosaki University
[3] Micro Analysis Laboratory, Tandem Accelerator, The University of Tokyo
[4] National Institute for Environmental Studies
[5] National Institute of Polar Research

identical for the LGM and early Holocene (uncorrected for post-depositional ^{36}Cl radioactive decay), being approximately 2.5–3.5 × 10^4 atoms cm^{-2} yr^{-1} (Fig. 1). These values are similar to the prospective nuclide flux at ~80 °S (~4–5 × 10^4 atoms cm^{-2} yr^{-1}), estimated from the latitudinal dependence of nuclide fallout [5] and the global mean production rate of ^{36}Cl [6, 7]. This similarity demonstrates the reliability of our measurements and the integrity of the ^{36}Cl record in the DF2 ice core. The ^{36}Cl flux at Greenland over the past 100 kyr was 5–10 × 10^4 atoms cm^{-2} yr^{-1} [8], which is 2–3 times higher than our values (Fig. 1). The reason for this discrepancy is currently unclear, but it probably reflects the different post-depositional behavior of chloride [9], and/or contrasting transport processes of the nuclide related to the characteristic tropospheric circulation regimes in the Northern and Southern Hemispheres.

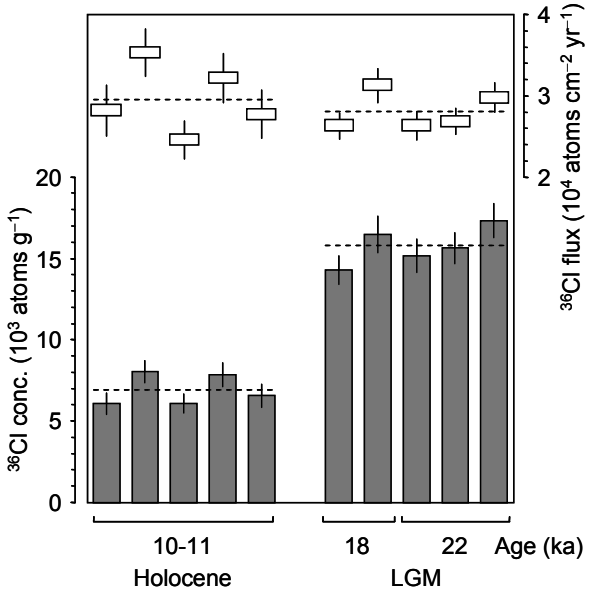

Fig. 1 Comparison of ^{36}Cl concentrations (gray bars) and depositional fluxes (open boxes) for the Last Glacial Maximum (LGM) and early Holocene at Dome Fuji Station, Antarctica. Error bars indicate ±1σ analytical uncertainty. Horizontal dashed lines represent averages for each period.

Acknowledgements

This work is supported in part by the Grants-in-Aid for Scientific Research Program of the Ministry of Education, Culture, Sports, Science and Technology, Japan.

References

[1] H. Motoyama, Scientific Drilling 5, (2007) 41–43.

[2] K. Kawamura et al., Nature 448 (2007) 912.

[3] K. Satow et al., Polar Meteorol. Glaciol., 13 (1999) 43-52.

[4] O. Watanabe, J. Jouzel, S. Johnsen, F. Parrenin, H. Shoji, N. Yoshida, Nature 422 (2003) 509.

[5] D. Lal, B. Peters, in: K. Sitte (Ed.), Handbuch der Physik, Vol. 46/2, Springer, Berlin, 1967, p. 551.

[6] J. Masarik, J. Beer, J. Geophys. Res. 104/D10 (1999) 12099.

[7] D. Huggle et al., Planet. Space Sci. 44 (1996) 147.

[8] S. Baumgartner et al., J. Geophys. Res. 102/C12 (1997) 26659.

[9] R.J. Delmas et al., Tellus 56B (2004) 492.

4.2 Measurement of ^{36}Cl in groundwater samples from Satsuma-Iwojima

Y. Tosaki, K. Sasa, T. Takahashi, Y. Matsushi[1], M. Tamari, T. Amano, K. Kazahaya[2], M. Yasuhara[2], H.A. Takahashi[2], N. Morikawa[2], M. Ohwada[2] and K. Asai[3]

Introduction

Chlorine-36 is an informative environmental tracer for determining the sources of chloride [1]. In order to distinguish one from other chloride sources, this application generally requires highly sensitive ^{36}Cl/Cl measurements, typically down to the order of 10^{-15}. This work therefore attempts to detect such low level ^{36}Cl/Cl in groundwater, and tests the applicability of our AMS (accelerator mass spectrometry) system. The eventual goal of this study is to investigate whether the application of ^{36}Cl can contribute to the understanding of groundwater systems under the influence of seawater and volcanic activity.

Study area and methods

Satsuma-Iwojima was selected as the study area, which is a volcanic island located at ~50 km south of Kyushu, southwestern Japan. This island constitutes the northwestern margin of the Kikai caldera formed after a large-scale eruption approximately 7,300 years ago [2,3]. The main largest aquifer exists in the middle of the island, exclusively offering drinkable groundwater [4]. During 28–29 November 2007, samples were collected from 9 wells within the main aquifer (samples Nos. 1–9) and 4 coastal hot springs around the island (Nos. 10–13).

Chloride concentrations were determined by ion chromatography at the Geological Survey of Japan. The ^{36}Cl/Cl ratios of the samples were measured with the AMS system at UTTAC. The sample volume for AMS ranged between 0.5 mL and 50 mL, corresponding to ~2 mg of Cl. Silver chloride (AgCl) was directly precipitated from each sample by using the standard method [5]. The background for the entire processes was evaluated with a process blank (halite sample), which gave a ^{36}Cl/Cl ratio of $(1.3 \pm 0.6) \times 10^{-15}$. The measured ratios were normalized to a ^{36}Cl standard (^{36}Cl/Cl = 1.60×10^{-12} [6]) and corrected for the background.

Results and discussion

Table 1 presents ^{36}Cl/Cl ratios and Cl^- concentrations in the samples. The obtained ratios were in the range of $1–6 \times 10^{-15}$. These low ratios might be attributed to the low meteoric ^{36}Cl/Cl ratios due to the close proximity of the sea. After recharge, there would be additional influences in aquifers by magmatic components and seawater. Figure 1 depicts the relationship between ^{36}Cl/Cl ratios and Cl^- concentrations. As an overall trend, the ^{36}Cl/Cl ratios decrease with increasing Cl^- concentration. Since the ^{36}Cl/Cl ratios in seawater and magmatic water are both expected to be very low (~1×10^{-15} or less) [7], the mixing of the Cl^- from these components with meteoric water could have resulted in isotopic dilution effects. This

[1] Micro Analysis Laboratory, Tandem accelerator, The University of Tokyo.
[2] Geological Survey of Japan, National Institute of Advanced Industrial Science and Technology
[3] Geo-Science Laboratory Co. Ltd.

reasonable trend supports the fundamental validity of the data presented here.

Figure 1 also shows several data points deviating from the mixing trend. Possible explanations include the difference in contribution of bomb-produced ^{36}Cl input (when the groundwater was recharged), which would be related to groundwater residence times. At present, however, we do not have enough data for further interpretation. When other geochemical and isotopic parameters are available, we will move on to a detailed discussion on the relationship between the ^{36}Cl data and the groundwater system.

References

[1] F.M. Phillips, in: P.G. Cook, A.L. Herczeg (Eds.), Environmental Tracers in Subsurface Hydrology, Kluwer, Boston, 2000, p. 299.

[2] K. Ono, T. Soya, T. Hosono, Geology of Satsuma-Io-Jima District, Geological Survey of Japan, Tsukuba, 1982 (in Japanese with English Abstract).

[3] H. Kitagawa, H. Fukuzawa, T. Nakamura, M. Okamura, K. Takemura, A. Hayashida, Y. Yasuda, Radiocarbon, 37 (1995) 371.

[4] K. Kazahaya, H. Shinohara, G. Saito, Programme and abstracts, the Volcanological Society of Japan, 1994-2 (1994) 218 (in Japanese).

[5] Y. Tosaki, N. Tase, G. Massmann, Y. Nagashima, R. Seki, T. Takahashi, K. Sasa, K. Sueki, T. Matsuhiro, T. Miura, K. Bessho, H. Matsumura, M. He, Nucl. Instr. and Meth. B 259 (2007) 479.

[6] P. Sharma, P.W. Kubik, U. Fehn, H.E. Gove, K. Nishiizumi, D. Elmore, Nucl. Instr. and Meth. B 52 (1990) 410.

[7] G.T. Snyder, U. Fehn, F. Goff, Earth Planet. Space 54 (2002) 265.

Table 1

Chloride concentrations and $^{36}Cl/Cl$ ratios in Satsuma-Iwojima samples

No.	Sample ID	Cl^- (mg/L)	$^{36}Cl/Cl$ (10^{-15})
1	SIJW_07_001	141	6.0 ± 1.2
2	SIJW_07_002	112	3.4 ± 1.2
3	SIJW_07_003	75.9	4.5 ± 1.1
4	SIJW_07_004	106	3.8 ± 1.1
5	SIJW_07_005	40.3	6.2 ± 1.0
6	SIJW_07_006	327	2.4 ± 0.9
7	SIJW_07_007	139	5.4 ± 1.1
8	SIJW_07_008	105	3.7 ± 1.1
9	SIJW_07_009	375	0.9 ± 0.8
10	SIJW_07_010	9978	3.9 ± 1.0
11	SIJW_07_011	1999	2.5 ± 0.9
12	SIJW_07_012	10066	1.0 ± 0.8
13	SIJW_07_013	1331	1.4 ± 0.8

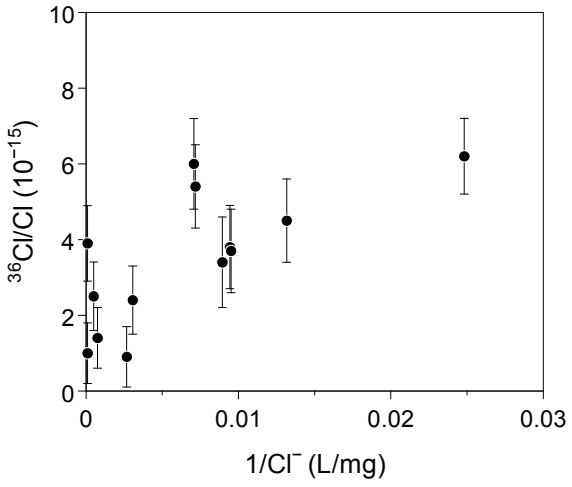

Fig. 1. $^{36}Cl/Cl$ ratios in the samples, plotted against reciprocal Cl^- concentrations.

4.3 Quantifying long-term limestone denudation using cosmogenic ^{36}Cl: an application to formative rate of a doline in the Akiyoshi karst, Japan

Y. Matsushi[1], K. Sasa, K. Sueki, T. Takahashi, T. Hattanji and Y. Matsukura

Introduction

Determination of denudation rates of land surfaces poses a fundamental issue in understanding landscape evolution over long timescales. Recent advances in the methodology using in situ-produced cosmogenic nuclides have brought innovation to strategies for quantifying denudation. Cosmogenic ^{36}Cl in calcite offers such a tool for carbonate rocks, providing an indicator of long-term physical and chemical mass loss from eroding surfaces [1]. Procedures for measuring cosmogenic ^{36}Cl and original Cl in rocks have already been developed at the University of Tsukuba Tandem Accelerator Complex (UTTAC) [2]. This paper reports an application of this method for a doline in the Akiyoshi karst composed of Mesozoic metamorphosed limestone, southeast Japan.

Samples and measurements

A small doline was selected (N34°15'35", E131°18'36", ~320 m a.s.l.) on the Akiyoshi-karst tableland. The doline exhibits a typical amphitheater-shaped depression with ~150 m in diameter and ~17 m in relative height. A north-south oriented cross section was surveyed, for which rock outcrops are available for sampling as many bare limestone pinnacles expose markedly along this direction. Samples were corrected at nine locations from the topmost ~5 cm of the pinnacles standing 50–140 cm high from its base. The nine sampling sites cover across the entire profile of the cross section (Fig. 1).

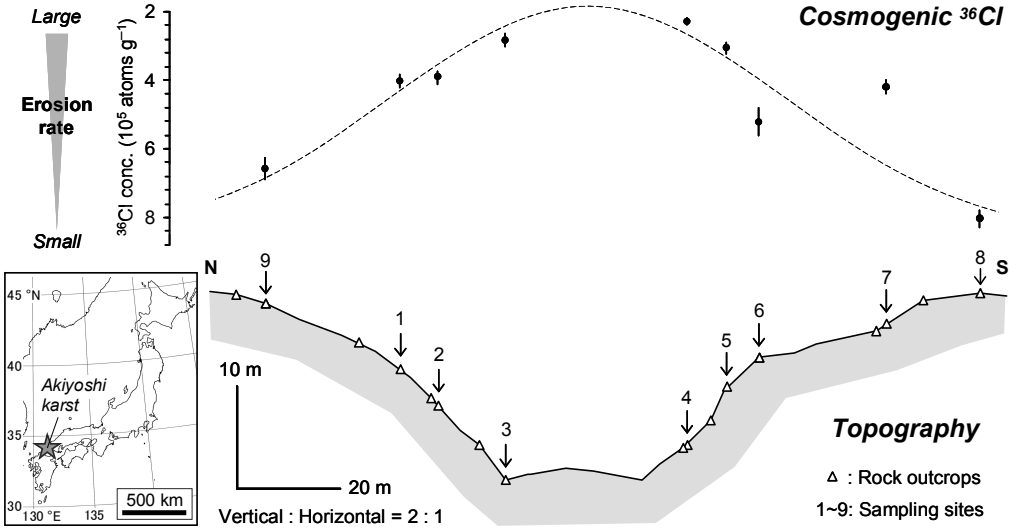

Fig. 1. Cosmogenic ^{36}Cl concentrations in limestone surfaces along a cross sectional profile of a doline in the Akiyoshi karst, Japan. Preliminary calculation indicates the denudation rates ranging from ~90 to ~25 mm kyr^{-1}, corresponding to the nuclide concentrations from 2×10^5 to 8×10^5 atoms g^{-1}, respectively.

[1] Micro Analysis Laboratory, Tandem accelerator, The University of Tokyo (*E-mail: matsushi@n.t.u-tokyo.ac.jp*).

Samples were prepared by a standard procedure for ^{36}Cl accelerator mass spectrometry (AMS) [2,3], and for Cl measurements by isotope dilution using a 99 atom%-enriched ^{35}Cl carrier from Aldrich Co. [2,4]. Simultaneous measurements of ^{36}Cl and Cl were carried out with the Tsukuba AMS System at UTTAC [5], by using an AMS-standard with the known ^{36}Cl/Cl ratio of 1.60×10^{-12} [6]. Concentration of Ca and abundances of other neutron absorption nuclei were determined for one of the nine samples (from site 1) by prompt gamma-ray analysis (PGA) with JRR-3M nuclear reactor at the Japan Atomic Energy Agency (JAEA).

Nuclide concentrations and denudation rates

Concentrations of ^{36}Cl in the samples range from 2×10^5 to 8×10^5 atoms g^{-1}, tending higher at upper parts, and lowest at bottoms of the slopes (Fig. 1). This tendency indicates that denudation rates are fastest at the center of the depression, and hence the doline has not reached a morphometric steady-state but is in-the process to be deepened.

Denudation rates of the limestone surfaces were calculated from the ^{36}Cl concentrations and nuclide production rates in calcite. The ^{36}Cl production rates were scaled preliminary through the calibrated spallogenic and muogenic nuclide production systematics [1,3,7], by using the latitude and elevation at the sites, and the measured chemical composition of the limestone: [Ca] = 39.2%, [Fe] = 0.2%, [Cl] = 4–9 ppm, [B] = ~0.4 ppm, [Sm] = ~0.3 ppm and [Gd] = ~0.3 ppm, with bulk density of 2.7 g cm^{-3}. The calculated denudation rates range from ~25 mm kyr^{-1} for the maximum ^{36}Cl concentration at the site 8 to ~90 mm kyr^{-1} for the minimum at the site 4, indicating 3−4 times higher rates at the bottom than at ridges of the doline.

The difference between the denudation rates is ~65 mm kyr^{-1}, and thereby the time needed for the formation of the relative height between the bottom and ridges (~17 m) is calculated to be about 260 kyr. During this duration, the doline experiences surface lowering of ~23 m at the center of the depression, and ~6.5 m even at the ridge with the lowest denudation. The difference in denudation rates may be attributed to nonuniform water supply, providing that the conditions of subsoil CO_2 and temperature are not much varied along the slopes. We are planning hydrological monitoring, including subsoil moisture contents as well as soil-air CO_2 concentrations and temperatures at the side slope of this doline, to explain mechanisms controlling the denudation rates of limestone surfaces linked to dynamic evolution of karst landforms.

References

[1] J.O.H. Stone et al., Geochim. Cosmochim. Acta 62 (1998) 433.
[2] Y. Matsushi et al., Nucl. Instr. and Meth. B in press.
[3] J.O. Stone et al., Geochim. Cosmochim. Acta 60 (1996) 679.
[4] D. Desilets et al., Chem. Geol. 233 (2006) 185.
[5] K. Sasa et al., Nucl. Instr. and Meth. B in press.
[6] P. Sharma et al., Nucl. Instr. and Meth. B 52 (1990) 410.
[7] J.O. Stone, J. Geophys. Res. 105 B10 (2000) 23753.

4.4 Production rates of ^{36}Cl for target elements in chondritic meteorites

Y. Hamanaka[1], Y. Oura[1], M. Ebihara[1], K. Sasa, Y. Nagashima, T. Takahashi, Y. Tosaki, Y. Matsushi, M. Tamari, T. Amano, K. Sueki, K. Bessho[2], N. Kinoshita[2]

Stable and radioactive cosmogenic nuclides, which are produced by nuclear reactions with high-energy cosmic rays during their flights in the space, provide important cosmochemical information. For example, several cosmogenic nuclides having different half life were determined simultaneously to be clear about complex cosmic-ray irradiation history [1]. ^{36}Cl is a one of the cosmogenic radionuclides and produced by several nuclear reactions such as proton and neutron induced spallation reactions (main target elements: K, Ca, Ti, Cr, Mn, Fe, and Ni) and neutron capture reaction (target nuclide: ^{35}Cl). Cross sections of those reactions are depended on particle energies characteristically. Thus it is suggested that additional information must be obtained from ^{36}Cl production rates normalized by a weight of target element (in dpm/kg) for individual target element. Therefore, we tried to determine production rates of ^{36}Cl in two chondritic meteorites in 2006 [2]. Further elemental production rates of ^{36}Cl were determined in another two meteorites in this study.

Two fragments of Gold Basin (L4 chondrite) and a fragment of Gao (H5 chondrite) were used in this sturdy. From powdered whole-rock samples, five phases with different elemental compositions were separated by both physical and chemical treatments. Chemical compositions of target elements for bulk and five separated phases samples were determined nondestructively by neutron induced prompt gamma-ray activation analysis (PGA) and instrumental neutron activation analysis. For analysis of ^{36}Cl by accelerator mass spectrometry (AMS), AgCl precipitates were prepared for each powder samples by a chemical process. ^{36}Cl/Cl ratios were determined by AMS at the Tandem Accelerator Complex, University of Tsukuba.

In Table 1, ^{36}Cl concentrations in separated phases of 3 fragments are shown. For all 3 fragments, silicate phases dissolved in nitric acid had highest ^{36}Cl concentration among bulk and 5 separated phases. These phases had also highest Cl concentrations and variations of Cl concentration among 6 phases in each fragment were significant in comparison with other target element concentrations except Co and Ni. Thus, experimentally, contribution of Cl to ^{36}Cl production in chondrites was proved qualitatively. Welten et al. [2] determined some cosmogenic nuclides including ^{36}Cl in 15 fragments of Gold Basin meteorite and estimated depth of those fragments in the pre-atmospheric meteoroid. According to the correlation between ^{36}Cl concentration and estimated depth, depths of fragment 1 and 2 in the meteoroid are estimated to be about 90 cm and 120 cm, respectively.

Production rates of ^{36}Cl for element groups, which are classified based on excitation function of proton induced spallation reaction, were calculated from ^{36}Cl concentrations and elemental abundances in bulk and separated phases, and shown in Table 2. It is noted that values in Table 2 are preliminary because Cl concentrations determined by PGA have a large uncertainty. Additional analysis of Cl by radiochemical

[1] Graduate School of Science and Engineering, Tokyo Metropolitan University
[2] Radiation Science Center, High Energy Accelerator Research Organization

photon activation analysis (RPAA) is planed to determine accurately. For Gold Basin meteorites, production rates for all element groups except Cl in fragment 1 are higher than those in fragment 2 and differences between fragments are varied according to element group. And the ratio of production rate for (K + Ca) to one for (Fe + Co + Ni + Mn) in fragment 2 is smaller than in fragment 1. As describing above, fragment 2 was estimated to be originated from deeper position in a meteoroid than fragment 1, which means that fragment 2 was irradiated by protons and/or secondary neutrons with smaller energy than fragment 1. Considering a feature of excitation functions on proton induced spallation reaction (with increase of production rate for Ca and Fe, a ratio of them decreases), the ratio of production rate in fragment 2 should be larger than in fragment 1. Calculated production rate for (K + Ca) in fragment 2 is guess to be too small. Relation of production rates between fragment 1 of Gold Basin and Gao seems to be reasonable. In contrast, production rates for Cl are similar among 3 fragments. Welten et al. [3] showed that concentrations of ^{36}Cl and ^{41}Ca produced by neutron capture in Gold Basin were dependent on depth. Therefore, after determining Cl concentration by RPAA, production rates will be calculated again, and further determination of ^{36}Cl in many fragments of Gold Basin is required.

Table 1 ^{36}Cl concentrations (dpm/kg) in separated phases.

	Gold Basin		Gao
phases	fragment 1	fragment 2	
bulk	10.9 ± 0.2	7.06 ± 0.14	9.95 ± 0.18
silicate	11.4 ± 0.2	5.47 ± 0.11	10.3 ± 0.2
metal	2.49 ± 0.07	1.33 ± 0.04	7.46 ± 0.15
insoluble in nitric acid	2.01 ± 0.06	1.23 ± 0.04	4.80 ± 0.13
soluble in nitric acid -1	46.8 ± 0.7	22.5 ± 0.3	25.3 ± 0.6
soluble in nitric acid -2	0.96 ± 0.03	0.74 ± 0.03	3.52 ± 0.08

Table 2 Production rates of ^{36}Cl in dpm/kgTarget.

	Gold Basin		Gao
target element group	fragment 1	fragment 2	
K + Ca	50	14	88
Ti + Cr	27	20	71
Fe + Co + Ni + Mn	2.1	0.88	7.6
Cl	25	28	28
(K + Ca) / (Fe + Co + Ni + Mn)	23	16	12

References

[1] M. Honda, K. Nishiizumi, M. Imamura, N. Takaoka, O. Nitoh, K. Horie, and K. Komura, *Earth Planet. Sci. Lett.* **57** (1982) 101.

[2] Y. Oura, S. Yamazaki, M. Ebihara, Y. Tosaki, K. Sasa, Y. Nagashima, T. Takahashi, Y. Tosaki, Y. Matsushi, M. Tamari, K. Sueki, H. Matsumura, K. Bessho, and T. Miura, *UTTAC Annural Report 2006* (2007) 39.

[3] K. C. Welten, M. W. Caffee, I. Leya, J. Masarik, K. Nishiizumi, and R. Wieler, *Meteorit. Planet. Sci*. **38** (2003) 157.

4.5 Chemical procedure for sulfur reduction for ^{36}Cl-AMS of soil samples

M. Tamari, K. Sueki, K. Sasa, T. Takahashi, Y. Tosaki, Y. Matsushi, T. Oki, T. Amano, Y. Nagashima, N. Kinoshita, H. Matsumura, K. Bessho

Introduction

Chlorine-36 is mainly measured through accelerator mass spectrometry (AMS), but ^{36}S, an isobar of ^{36}Cl, interferes with the measurement. In surface soil, sulfur is mainly present as organic sulfur [1]. When extract is added to the soil, not only an inorganic substance but also a part of organic substance is extracted and the usual method of removing sulfate ions from samples—the $BaSO_4$ precipitation method—is ineffective in removing extractable organic sulfur. We developed new leaching procedures for removing the organic sulfur from the soil.

The sample for measurement of the isotope ratio (^{36}Cl/Cl) in all chlorine can be obtained by burning and collecting whole soil as pre-treatment. By the measurement from inorganic chlorine and organic chlorine, an inorganic substance was extracted from the soil at first, and it is attained by making residue burning and taking out chlorine. A method is established that an inorganic substance without sulfur is taken out from the soil and is measured by accelerator mass spectrometry (AMS).

Examination of leaching procedure for soil

Two kinds of soil were used in this study. One was surface soil collected at the University of Tsukuba (Tsukuba soil), and was applied to examine the degree of interference of ^{36}S after different leaching processes. Another was uncultivated surface soil collected at Tokai-mura (Tokai soil), and was applied to examine the ^{36}Cl/Cl ratios after different leaching processes.

The leaching conditions for Cl are shown in Figure 1. Soil was dried up at 120°C, and was sieved to eliminate >2 mm-size particles. Extractant (ultrapure water, 0.01 M HNO_3 or 0.8 M HNO_3 with 1.5-5 times the weight of the dried soil) was added to the soil. Then, in Tsukuba E, F and Tokai L, 30% H_2O_2 was used to decompose the organic matter in soil (ratios of H_2O_2 to dried soil: 15 ml/100 g, 170 ml/100 g, and 100 ml/100 g, respectively). Supernatant was separated from the soil by centrifugation. In Tokai I and K, 1-1.5 g of activated carbon (Calgon Mitsubishi Chemical Corporation) was added to the supernatant in order to remove extractable organic matters without decomposition. The organic matter in the solution was decomposed with 30% H_2O_2 (10-30 ml) in each procedure except Tsukuba A, C, E and F. After leaching from soils, the AgCl samples for AMS-target made from the obtained solutions at ordinary treatment.

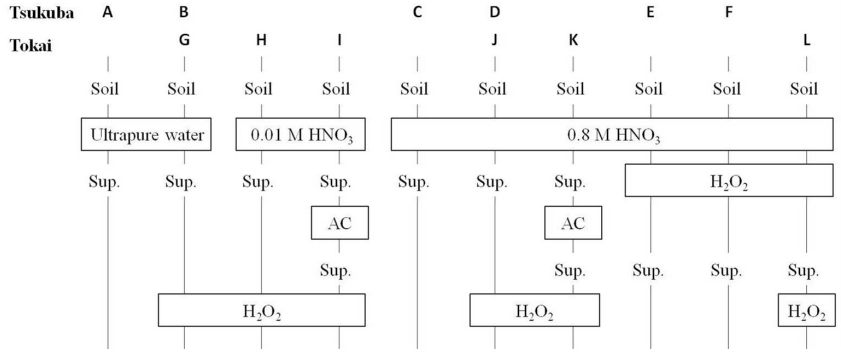

Figure 1. Leaching procedures for soil samples. (AC and Sup. mean activated carbon and supernatant.) (See [2] for more on Tsukuba C.)

Results and discussion

The results of ^{36}S-assay and ^{36}Cl-AMS are shown in Table 1, as well as those of the standard samples (^{36}Cl/Cl = 1.000×10^{-11} [11]). The ^{36}S-assay shows the counts per second of ^{36}S in the detector and the degree of interference of ^{36}S indicated by ^{36}S/^{35}Cl ratio. In Tsukuba A, neither ^{36}Cl nor ^{36}S were counted because of large interference from ^{36}S. In the same extractant the addition of H_2O_2 to the sample (Tsukuba B, D) reduced the interference from ^{36}S to lesser than that for the samples without H_2O_2 (Tsukuba A, C). In Tsukuba E and F, the extractant and H_2O_2 added directly in the soils, but in Tsukuba E in which too little H_2O_2 was used so that the decomposition reaction was only half completed, there was large ^{36}S interference. The result was shown that the interference from ^{36}S reduced Tsukuba D and F by using diluted HNO_3 as extractant, and H_2O_2 sequentially.

Table 1 Results of ^{36}S-assay and ^{36}Cl-AMS for soil samples

Sample	^{36}S/^{35}Cl ×10^{2} (counts/μC)	^{36}S ×10^{3} (cps)	^{36}Cl/Cl ×10^{-13} (atoms/atoms)
Tsukuba A*	-	> 6.6	-
Tsukuba B	2.2	1.4	1.07 ± 0.11
Tsukuba C	4.1	2.0	2.92 ± 0.50
Tsukuba D	0.5	0.4	0.94 ± 0.05
Tsukuba E	13.2	6.6	1.28 ± 0.20
Tsukuba F	0.5	0.4	1.08 ± 0.06
Tokai G	2.2	1.2	149 ± 4
Tokai H	1.1	0.6	125 ± 10
Tokai I	0.3	0.2	145 ± 3
Tokai J	1.7	0.2	129 ± 11
Tokai K	0.9	0.6	144 ± 15
Tokai L	2.0	1.0	79 ± 3
STD†	0.07-1.6	0.06-1.4	100

* Detection did not work because of a large interference of ^{36}S.
† Standard for ^{36}Cl-AMS (^{36}Cl/Cl = 1.000 × 10^{-11})

We examined the differences in the ^{36}Cl/Cl ratios among the different leaching procedures in Tokai soil, which had a ^{36}Cl/Cl ratio of order 10^{-11}. Within system error, the ^{36}Cl/Cl ratios were almost the same except for Tokai L, and that for Tokai L was about half of the others. However, the ratios for Tokai H (J) seem slightly lower than for Tokai I (K). This suggests that the ^{36}Cl/Cl ratio for Tokai L became lower than those of the others due to the decomposition of the organic chlorine. In other words, the ^{36}Cl/Cl ratio for organic chlorine seems to be lower than that for inorganic chlorine in Tokai soil.

References

[1] G.E. Likens et al., Biogeochemistry 60 (2002) 235.

[2] R. Seki et al., Nucl. Instr. and Meth. B 259 (2007) 486.

5.

INTERDISCIPLINARY RESEARCH

5.1 Nucleation rate of nano-particles in $N_2/H_2O/SO_2$ by 20 MeV protons

S. Tomita, M. Fujieda, M. Matsuoka, K. Terada, K. Sasa, H. Kudo

Formation mechanism of nano-particles in gas mixture of $N_2/H_2O/SO_2$ at atmospheric pressure attract attentions, because this might explain a possible correlation between the Earth's total low-altitude cloud cover and galactic cosmic ray flux [1]. Under proton irradiation, H_2SO_4 is formed by oxidation reaction of SO_2 with OH radicals which produced by the energetic protons. The H_2SO_4 plays an important role in nucleation process, and produces nano-partiles with diameter of about 8 nm.

In this report, we report nano-particle formation rate as a function of proton beam intensity. The experiments were performed with a tandem accelerator (12UD Pelletron) at University of Tsukuba. The size distribution of nano-particle was obtained by measuring the electrical mobility of charged particle with a differential mobility analyzer. The density of produced nanoparticles was then obtained by integrating the area under the spectrum. Figure 1 shows a typical result obtained for the sample gas 0.2 ppm SO_2, 80% relative humidity. It is clearly seen that the droplet yield is proportional to the square root of beam intensity. Since almost all of the ions produced by the proton beam is recombined and become neutral, the resulted ion density becomes proportional to the square root of proton beam intensity. Therefore, one can say that the droplet yield is proportional to the ion density generated by proton beam. This shows possible importance of ions for the nucleation process. As written above, H_2SO_4 is important for the nucleation process. Thus, ions might play important role in the oxidation mechanism or the nucleation process. Further investigations are planned to ensure the possibilities.

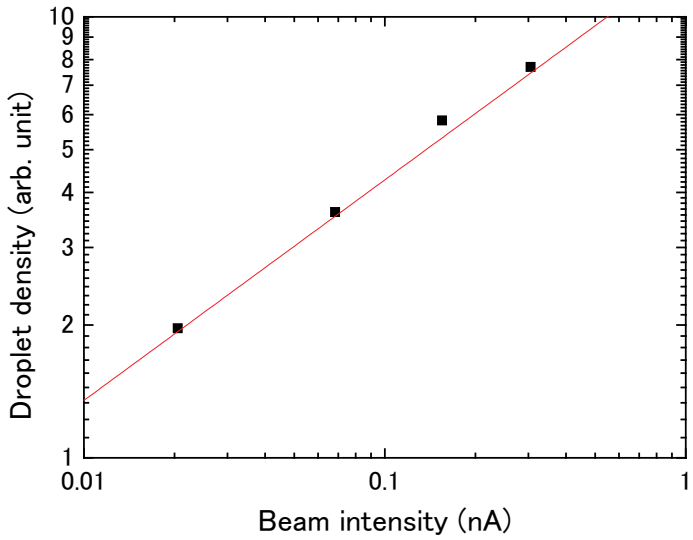

Fig.1. Densities of generated water droplet as a function of proton beam intensities. The sample gas was $N_2/H_2O/SO_2$, with relative humidity of 80% and SO_2 concentration of 0.2 ppm. Solid line shows power of 0.5.

References

[1] N.D. Marsh, and H. Svensmark, Phys. Rev. Lett. **85**, 5004 (2000).

5.2 Open Advanced Facilities Initiative for Innovation (strategic use by industry) at UTTAC

H. Kudo, Y. Tagishi, H. Naramoto, S. Mihara, T. Oki

In the fiscal years 2007-2008, UTTAC provided 20-25% of the available machine time for industrial researches programmed by ~10 industries, which were supported by the Open Advanced Facilities Initiative for Innovation conducted by The Japanese Ministry of Education, Culture, Sports, Science and Technology (MEXT) [1]. The background of this program includes new mission required currently for universities in Japan, i.e., social contribution, in addition to the main mission of education and fundamental research.

The researches include ion beam analysis of materials, ion beam fabrications, ion irradiation experiments, and material analysis using radioisotopes. The list of the research programs are shown in Table 1, which were reviewed and accepted by the steering committee organized for the initiative. The research results for the finished programs have been or are to be published in the home page of MEXT [2].

Table 1. List of the research programs

Research title: Industry	FY2007	FY2008	FY2009	FY2010
Development of radiation detector for use on satellite: Meisei Electric + JAXA				
[Test exp.] Study of durability test for public-use semiconductor devices using low-LET particle beams: Mitsubishi Electric + Ryoei Technica	finished			
Development of high sensitivity sensors using nano perforation with swift heavy ion irradiation: Emerging Technologies Corporation		finished		
Analysis of hydrogen in thin films: Optical instrument maker				
Preliminary search for a raremetal deposit related with radioisoropes: Developer of mineral resources			finished	
[Test exp.] Analysis of impurities in semiconductor crystals: R&D Association for Future Electron Devices		finished		
Characterization of nonorganic films by high-energy ion beams: general beverage maker				
Mossbauer study of electron states of nanoparticles: General electric maker				
PIXE analysis of impurities in SiC: R&D Association for Future Electron Devices			finished	
Hydrogen analysis in electronic devices: Electronic device maker				
Study of characterization technique for public-use semiconductor devices using low-LET particle beams: Mitsubishi Electric + Ryoei Technica				

References

[1] This report was published on June 15, 2009 (Vol. 5, No. 6) in the online journal, "Journal of Industry-Academia-Government Collaboration" http://sangakukan.jp/journal/index.html, published (in Japanese) monthly by Japan Science and Technology Agency (JST).

[2] http://kyoyonavi.mext.go.jp/report/search

5.3 Micro-PIXE analyses of fluid inclusions in quartz from miarolitic cavities at the Kofu granite, Japan

M. Kurosawa, S. Ishii and K. Sasa

Introduction

Fluid released from granitic magma during solidification plays a key role in many geological events related to hydrothermal process. Compositions of the granite-derived fluid are commonly approximated by the H_2O–CO_2–NaCl system, and the fluid also has wide varieties of other elemental species and concentration range [1]. Thus, it is essential to formation of various metal-ore deposits, hydrothermal alteration, and chemistries of deep groundwater inside and around granite bodies [1]. A part of the fluid is normally trapped as fluid inclusions in the solidified granite and surrounding rocks. Chemical analyses of the inclusions, therefore, provide abundant information about chemistries and behaviors of the fluid. Fluid inclusions in minerals from miarolitic cavities inside granite are particularly important to investigate an original composition of fluids released during solidification of the granite. Because miarolitic cavities are commonly formed by entrapment of fluid segregated by vesiculation of granite magma during the final stage of crystallization of the granite. Hence, fluid inclusions of quartz crystals in miarolitic cavities from granites at the continental area have been analyzed by particle-induced X-ray emission (PIXE) and laser ablation-inductively coupled plasma-mass spectrometry [2-5]. The analytical results for the island-arc granite, however, are very scarce. For these reasons, we describe micro-PIXE analyses of single fluid inclusions in quartz crystals from miarolitic cavities at the Kofu granite, Japan.

Sample

Miarolitic cavities are common in biotite granite of the Miocene Kofu granite body near Kurobera district, Kofu, Yamanashi Prefecture. Localities of four cavities used in this study are very close, a distance of less than 3 km. These cavities are a few to tens cm in diameter, consists of smoky quartz, microcline, albite, muscovite, and a small amount of schorl. They are sometimes accompanied by small amounts of topaz, zinnwaldite, beryl, monazite-(Ce), and cassiterite. Smoky euhedral quartz crystals were collected from these miarolitic cavities for the inclusion analyses. Fluid inclusions in the quartz samples are two-phase inclusions, 70–120 μm in size (Fig. 1). The homogenization temperatures range from about 380 to 280°C and have a peak around 350°C. Measured inclusions were an ellipsoidal or negative-crystal shape, and the inclusion depths were less than 10 μm.

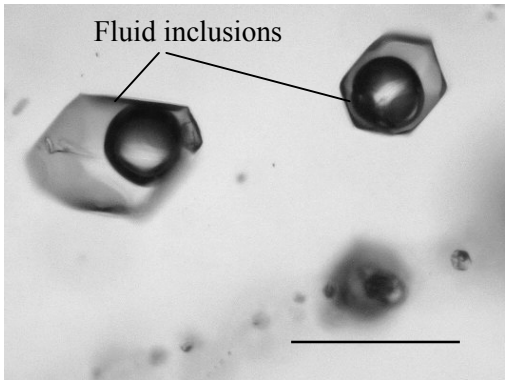

Fig.1. Photomicrograph of fluid inclusions in quartz crystal from a miarolitic cavity at the Kofu granite, Japan. Large bubbles are present in the inclusions. Scale bar is a 100 μm.

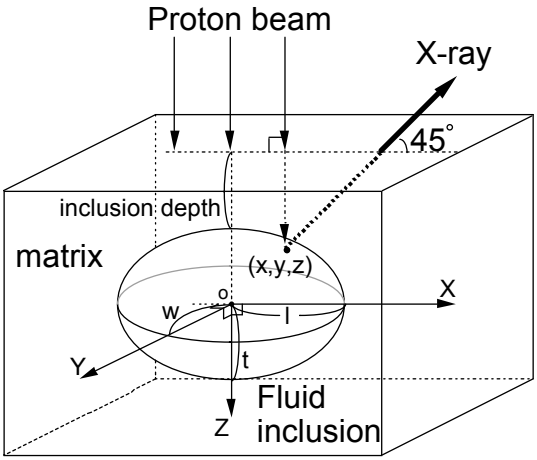

Fig.2. Schematic geometry for PIXE analysis of fluid inclusion.

Experimental

The PIXE analyses were performed at the 1MV Tandetron. A 1.0 to 5.0 nA beam of 1.92-MeV proton was focused to a 100 x 100 μm spot on the sample using slits and magnetic lenses. The beam incidence was normal to the sample surface, and the X-ray measurement take-off angle was 45˚[6]. The characteristic X-rays excited by the incident beam were collected by the Si(Li) X-ray-energy detector (Gresham Co.) with a nominal resolution of 153 eV at 5.9 keV. A 55-μm-thick Mylar film was used to attenuate the intense X-rays from the predominant light elements and to prevent the entry into the detector of protons scattered from samples. The total charge was determined by integrating the target currents, and all samples were analyzed to the integrated charges of 0.5 to 5.0 μC. Analytical points were chosen based on optical viewing using a CCD camera mounted on the microscope [6]. Quantification was performed based on the model of Kurosawa et al. [7,8]. Intensities of X-rays generated from fluid inclusions are decreased by the attenuation of energy of the incident protons and the absorption of the X-rays by a quartz matrix and the fluid, because fluid inclusions are buried in the matrix (Fig. 2). In this model, the decrease of total X-ray intensities from a whole fluid-inclusion are calculated by considering sizes and depth of fluid inclusion, the major element composition, the densities of the matrix and the fluid, their proton-stopping powers, the X-ray production cross sections, and the X-ray absorption coefficients. Finally, element concentrations are calculated based on X-ray intensities corrected for the decrease and the detector sensitivity determined for each element. A shape of the fluid inclusion is assumed as an ellipsoidal equal to the size of the measured fluid inclusion. The inclusion sizes were determined with an optical microscope. The inclusion depths were exactly determined by measuring an intensity ratio of Cl K_α and Cl K_β. In the calculations, contributions of X-rays from impurities in the matrix and bubbles in the fluid inclusion were also corrected [7,8]. By using the calculation model, almost trace elements in fluid inclusions at levels of a few to several thousands ppm can be determined with the total analytical error of θ11- 40 % [7].

Results and Discussion

PIXE spectra of a fluid inclusion in the miarolitic cavities consisted of K X-ray peaks from Cl, K, Ca, Mn, Fe, Cu, Zn, Ge, Br, and Rb, and of L X-ray peaks from Pb and Ba (Fig. 3). Most of inclusions in the miarolitic cavities demonstrated the similar X-ray spectra. The element concentrations determined were several tens to hundreds of wt. ppm for Mn, Fe, Cu, Zn, Rb, Ge, Ba, and Pb. For the inclusions, calculated salinities range from about 8 to 17 wt.% NaCl equivalent: they were calculated based on the assumption that all the chlorine contents are originated from NaCl components. The fluid inclusions of the miarolitic cavities are divided into two types: low-content type with tens of ppm for the most

transition-metal elements and high-content types with hundreds of ppm for those. Although a quartz crystal in the single miarolitic cavities basically contained inclusions of the one type, both type of inclusions were rarely observed in the same crystals of the particular cavity. Compositions of all the inclusions showed positive correlations between Mn and Fe, Zn and Fe, Zn and Cu, Ge and Zn, Ba and Zn, and Pb and Zn concentrations. The interelement ratios (e.g., Mn/Fe and Ge/Zn) of the both type of inclusions are nearly constant at a level well within the analytical error. Thus, the compositional difference in both types of inclusions could not be due to inflow of different magmatic fluids but due to dilution of magmatic fluids by meteoritic waters during formation of the miarolitic cavities. Fluid inclusions in single quartz crystals from miarolitic cavities at the continental area have often demonstrated extreme variations in elemental concentration, ranging over several orders of magnitude [2-5]. These variations suggest chemical diversity of magmatic fluids during granite solidification. Lack of the extreme variations for the present samples indicates that an original fluid generated during the granite solidification could be formed by relatively simple processes, unmixing of fluids from granitic magma and the dilution by meteoritic water. Further chemical variation of the fluid would be caused by secondary processes during and after transport of the fluid inside the granite body.

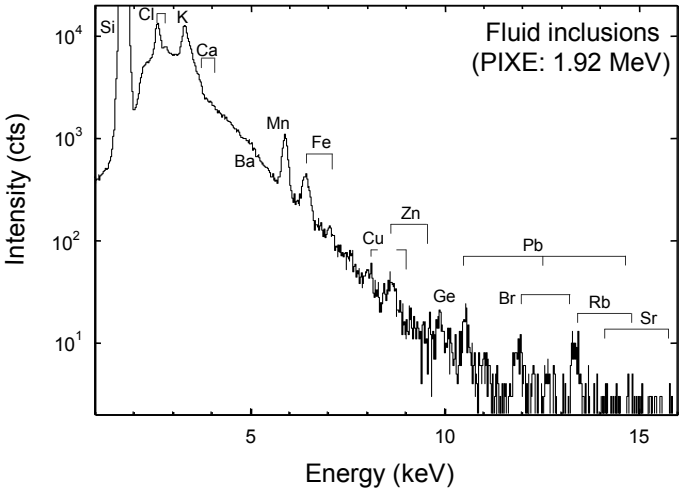

Fig.3. PIXE spectrum of fluid inclusion in quartz crystal from miarolitic cavity at the Kofu granite, Japan.

References

[1] E. Roedder, Rev. Mineral., 14, "Fluid Inclusions" (1984)

[2] A. Audétat et al., Science, 279 (1998) 2091.

[3] A. Audétat et al., Econ. Geol., 95 (2000) 1563.

[4] V. S. Kamenetsky et al., Geology, 30 (2002), 459.

[5] V. S. Kamenetsky et al., Chem. Geol., 210 (2004), 73.

[6] M. Kurosawa et al., Nucl. Instr. and Meth. B142 (1998), 599.

[7] M. Kurosawa et al., Geochim. Cosmochim. Acta, 67 (2003), 4337.

[8] M. Kurosawa et al., Nucl. Instr. and Meth. B266 (2008), 3633.

6. LIST OF PUBLICATIONS

The publications listed here are those released in the fiscal year 2008 by all the workers listed on p.46.

6.1 Journals

NUCLEAR PHYSICS

1. T. Yamaguchi, T. Suzuki, T. Ohnishi, F. Becker, M. Fukuda, H. Geissel, M. Hosoi, R. Janik, K. Kimura, T. Kuboki, S. Mandel, M. Matsuo, G. Münzenberg, S. Nakajima, T. Ohtsubo, A. Ozawa, A. Prochazka, M. Shindo, B. Sitár, P. Strmeň, T. Suda, K. Sümmerer, K. Sugawara, I. Szarka, M. Takechi, A. Takisawa, K. Tanaka, and M. Yamagami, Nuclear matter radii of neutron-deficient Kr isotopes, Physical Review C 77, 034315 (2008).

2. Tetsuya Ohnichi, Toshiyuki Kubo , Kensuke Kusaka, Atsushi Yoshida, Koichi Yoshida, Naoki Fukuda, Masao Ohtake, Yoshiyuki Yagagisawa, Hiroyuki Takeda, Daisuke Kameda, Yoshitaka Yamaguchi, Nori Aoi, Ken- ichiro Yoneda, Hideaki Otsu, Satoshi Takeuchi, Takashi Sugimoto, Yosuke Kondo, Heiko Scheit, Yasuyuki Gono, Hiroyoshi Sakurai, Tohru Motobayashi, Hiroshi Suzuki, Taro Nakao, Hitomi Kimura, Yutaka Mizoi, Masafumi Matsushita, Kazuo Ieki, Takamasa Kuboki, Takayuki Yamaguchi, Takeshi Suzuki, Akira Ozawa, Tetsuaki Moriguchi, Yusuke Yasuda, Takashi Nakamura, Takashi Nannichi, Tomoyuki Shimamura, Yoshiaki Nakayama, Hans Geissel, Helmut Weick, Jerry A. Nolen, Oleg B. Tarasov, Anthony S. Nettleton, Daniel P. Bazin, Bradley M. Sherrill, David J. Morrissey, and Wolfgang Mittig, Identification of New Isotopes ^{125}Pd and ^{126}Pd Produced by In-Flight Fission of 345 MeV/nucleon ^{238}U: First Results from the RIKEN RI Beam Factory, Journal of the Physical Society of Japan, Vol. 77, No. 8, August, (2008) 083201.

3. Y.Yamaguchi, A.Ozawa, A.Goto, I.Arai, T.Fujinawa, N.Fukunishi, T.Kikuchi, T.Ohnishi, T.Ohtsubo, H.Sakurai, T.Suzuki, M.Wakasugi, T.Yamaguchi, Y.Yasuda, Y.Yano, Rare-RI ring project at RIKEN RI beam factory, Nuclear Instruments and Methods in Physics Research B 266, 4575-4578 (2008).

4. S.Nakajima, T.Kuboki, M.Yoshitake, Y.Hashizume, M.Kanazawa, A.Kitagawa, K.Kobayashi, T.Moriguchi, T.Ohtsubo, A.Ozawa, S.Sato, T.Suzuki, Y.Yamaguchi, Y.Yasuda. T.Yamaguchi, Development of a time-of-flight detector for the Rare-RI Ring project at RIKEN, Nuclear Instruments and Methods in Physics Research B 266, 4621-4624 (2008).

5. B.Sun, R.Knöbel, Yu.A.Litvinov, H.Geissel, J.Meng, K.Beckert, F.Bosch, D.Boutin, C.Brandau, L.Chen, I.J.Cullen, C.Dimopoulou, B.Fabian, M.Hausmann, C.Kozhuharov, S.A.Litvinov, M.Mazzocco, F.Montes, G.Münzenberg, A.Musumarra, S.Nakajima, C.Nociforo, F.Nolden, T.Ohtsubo, A.Ozawa, Z.Patyk, W.R.Plaβ, C.Scheidenberger, M.Steck, T.Suzuki, P.M.Walker, H.Weick, N.Winckler, M.Winkler, T.Yamaguchi, Nuclear structure studies of short-lived neutron-rich nuclei with the

novel large-scale isochronous mass spectrometry at the FRS-ESR facility, Nuclear Physics A 812 (2008) 1-12

6. A.Ozawa, D.Q.Fang, M.Fukuda, N.Iwasa, T.Izumikawa, H.Jeppesen, R.Kanungo, R.Koyama, T.Ohnishi, T.Ohtsubo, W.Shinozaki, T.Suda, T.Suzuki, M.Takahashi, I.Tanihata, C.Wu, Y.Yamaguchi, Measurement of the reaction cross section of 18C and observations of fragments from ^{17}C and ^{18}C at 80 AMeV, Physical Review C 78, 054313 (2008).

7. C.B. Moon, C.S. Lee, M. Oshima, Y. Toh, J. Goto, Y. Hatsukawa, A. Kimura, M. Koizumi, A. Osa, T. Komatsubara, K. Miyakawa, Multi-quasiparticle states in odd-odd I-118, Journal of the Korean Physical Society, Vol. 53, No. 4, October (2008) 1844-1847

8. T. Shizuma, T. Hayakawa, H. Ohgaki, H. Toyokawa, T. Komatsubara, N. Kikuzawa, A. Tamii, H. Nakada, Fine structure of the magnetic-dipole-strength distribution in Pb-208, Phys. Rev. C 78, 061303, Dec (2008)

MATERIALS AND CLUSTER SCIENCE

9. Eiji Kita, H. Yanagihara, S. Hashimoto, K. Yamada, T. Oda, M. Kishimoto, and A. Tasaki, Hysteresis Power-Loss Heating of Ferromagnetic Nanoparticles Designed for Magnetic Thermoablation, IEEE Trans MAG, MAG44 No.11 part2, pp. 4452-4455 (2008).

10. Takahiro Kondo, Ken-ichi Izumi, Kenji Watahiki, Yosuke Iwasaki, Tetsuya Suzuki and Junji Nakamura, Promoted catalytic activity of a Platinum monolayer cluster on Graphite, Journal of Physical Chemistry C, Vol. 112, 15607-15610, 2008

11. JunePyo Oh, Takahiro Kondo, Daigo Hatake and Junji Nakamura, Elastic and inelastic scattering components in the angular intensity distribution of He scattered from graphite, Surface Science, Vol. 603, 894-899, 2009

12. H. Sano M. Miyaoka, T. Iimori, D. Sekiba, K. Nakatsuji, W. Wolf, R. Podloucky, N. Kawamura, G. Mizutani, F. Komori, Enhancement of optical second harmonic generation bynitrogen adsorption on Cu(001), Appl. Surf. Sci.255, (2008) 3289-3293.

13. Kan Nakatsuji, Yoshihide Yoshimoto, Daiichiro Sekiba, Shunsuke Doi, Takushi Iimori, Kazuma Yagyu, Yasumasa Takagi, Shin-ya Ohno, Hideharu Miyaoka, Masamichi Yamada, Fumio Komori, Kenta Amemiya, Daiju Matsumura, and Toshiaki Ohta, Electron correlation effects in Co nanoscale islands on a nitrogen-covered Cu(001) surface, Phys. Rev. B 77 (2008) 235436-1-8.

14. Kan Nakatsuji, Takushi Iimori, Yasumasa Takagi, Daiichiro Sekiba, Shunsuke Doi, Masamichi Yamada, Taichi Okuda, Ayumi Harasawa, Toyohiko Kinoshita, Fumio Komori, Surface restructuring process on a Ag/Ge(0 0 1) surface studied by photoelectron spectroscopy, Applied Surface Science, 254 (2008) 7638-7641.

15. D. Sekiba, H. Yonemura, T. Nebiki, M. Wilde, S. Ogura, H. Yamashita, M. Matsumoto, J. Kasagi, Y. Iwamura, T. Itoh, H. Matsuzaki, T. Narusawa, K. Fukutani, Development of microbeam NRA for 3D-mapping of hydrogen distribution in solids: Application of tapered glass capillary to 6 MeV 15N ion, Nuclear Instruments and Methods in Physics Research Section B: Beam Interactions with Materials and Atoms, Volume 266 (2008) 4027-4036.

16. T. Nebiki, D. Sekiba, H. Yonemura, M. Wilde, S. Ogura, H. Yamashita, M. Matsumoto, K. Fukutani, T. Okano, J. Kasagi, Y. Iwamura, T. Itoh, S. Kuribayashi, H. Matsuzaki, T. Narusawa, Taper angle dependence of the focusing effect of high energy heavy ion beams by glass capillaries, Nuclear Instruments and Methods in Physics Research Section B: Beam Interactions with Materials and Atoms, 266 (2008) 1324-1327.

17. D. Sekiba, Y. Yoshimoto, K. Nakatsuji, F. Komori, Lattice strain and related phenomena on Metal Surfaces (in Japanese), Journal of the Vacuum Society of Japan, 51 (2008) 285.

18. A. Uedono, C. Shaogiang, S. Jongwon, K. Ito, H. Nakamori, N. Honda, S. Tomita, K. Akimoto, H. Kudo, and S. Ishibashi, Vacancy-type defects in Er-doped GaN studied by a monoenergetic positron beam, J. Appl. Phys. 103, (2008) 104505 (1-5)

19. Masataka Ohkubo, Masahiro Ukibe, Yiner Chen, Shigetomo Shiki, Yuki Sato, Shigeo Tomita, Shigeo Hayakawa, Superconducting Solid-State Particle Spectrometers for Atoms and Macromolecules of 3-20 keV, J. Low. Temp. Phys. 151, (2008) 760-765

20. S. Shiki, M. Ukibe, Y. Sato, S. Tomita, S. Hayakawa, M. Ohkubo, Kinetic-energy-sensitive mass spectrometry for separation of different ions with the same m/z value, J. Mass Spectro. 43, (2008) 1686-1691

21. S. Shiki, M. Ukibe, R. Maeda, M. Ohkubo, Y. Sato, S. Tomita, Energy resolution improvement of superconducting tunnel junction particle detectors with infrared-blocking filters, Nucl. Instrum. and Methods A-595, (2008) 391-394

ACCELERATOR MASS SPECTROMETRY

22. M. Hoshi, S. Endo, K. Tanaka, M. Ishikawa, T. Straume, K. Komura, W. Rühm, E. Nolte, T. Huber, Y. Nagashima, R. Seki, K. Sasa, K. Sueki, H. Fukushima, S. D. Egbert and T. Imanaka, Intercomparison study on ^{152}Eu gamma ray and ^{36}Cl AMS measurements for development of the new Hiroshima-Nagasaki Atomic Bomb Dosimetry System 2002 (DS02), Radiation and Environmental Biophysics, 47 (2008) 313-322.

INTERDISCIPLINARY RESEARCH

23. S.C.B. Gopinath, K. Awazu, M. Fujimaki, K. Sugimoto, Y. Ohki, T. Komatsubara, J. Tominaga, K.C. Gupta, P.K.R. Kumar, Influence of nanometric holes on the sensitivity of a waveguide-mode sensor: Label-free nanosensor for the analysis of RNA aptamer-ligand interactions, Analytical Chemistry, Vol. 80, Sep (2008), 6602-6609

24. M. Fujimaki, C. Rockstuhl, X.M. Wang, K. Awazu, J. Tominaga, Y. Koganezawa, Y. Ohki, T. Komatsubara, Silica-based monolithic sensing plates for waveguide-mode sensors, Optics Express, Vol. 16, 6408-6416, Apr (2008)

25. T. Komatsubara, K. Sasa, H. Ohshima, H. Kimura, Y. Tajima, T. Takahashi, S. Ishii, Y. Yamato, M. Kurosawa, Hydrogen analysis for granite using proton-proton elastic recoil coincidence spectrometry, Radiation and Environmental Biophysics 47 (2008) 337-342

26. K. Awazu, X. Wang, M. Fujimaki, J. Tominaga, H. Aiba, Y. Ohki, T. Komatsubara, Elongation of gold nanoparticles in silica glass by irradiation with swift heavy ions, Phys. Rev. B 78, 054102 (2008)

27. I. Sugai, Y. Takeda, M. Oyaizu, H. Kawakami, K.Sasa, S. Ishii, K. Shima, First results of target preparation by the HIVIPP method in pressures higher than one bar, Nuclear Instruments and Methods in Physics Research A, 590 (2008) 83-90.

28. Masanori Kurosawa, Satoshi Ishii and Kimikazu Sasa, Quantitative PIXE analyses of single fluid inclusions in quartz crystals with a 1.92-MeV tandetron, Nuclear Instruments and Methods in Physics Research B, 266 (2008) 3633-3642.

29. Seung-Jun Yu, Yoshimichi Ohki, Makoto Fujimaki, Koichi Awazu, Junji Tominaga, Kimikazu Sasa and Tetsuro Komatsubara, Reduction in Polarization Dependent Loss of a Planar Lightwave Circuit by Ion-implantation-induced Birefringence, Nuclear Instruments and Methods in Physics Research B, 266 (2008) 4762-4765.

6.2 International conferences

1. Junji Nakamura, Takahiro Kondo, Ken-ichi Izumi, Kenji Watahiki, Yosuke Iwasaki, June Pyo Oh, Daiichiro Sekiba, Hiroshi Kudo, Catalytic property and morphology of Pt clusters on the graphite surface, The 5th International Symposium on Surface Science and Nanotechnology (ISSS-5), Waseda (Tokyo) 9-13, November, 2008.

2. D. Sekiba, H. Yonemura, Y. Kitaoka, M. Matsumoto, Y. Iwamura, T. Itoh, H. Matsuzaki, T. Narusawa, K. Fukutani, In-situ NRA measurement of hydrogen uptake in palladium foil, 4th Vacuum and Surface Sciences Conference of Asia and Australia, Matsue (Japan) 28-31 October, 2008.

3. Takahiro Kondo, Kenji Watahiki, June Pyo Oh, Ken-ichi Izumi, Yosuke Iwasaki, Daiichiro Sekiba, Hiroshi Kudo and Junji Nakamura, Catalytic Activity and Morphology of Pt Clusters on the Graphite Surface, American Vacuum Society (AVS) 55th International Symposium, Boston (United States) 19-24, October, 2008.

4. June Pyo Oh, Takahiro Kondo, Yoshiyuki Suda, Daiichiro Sekiba, Hiroshi Kudo and Junji Nakamura, Significant Reduction in Adsorption Energy of CO on Platinum Nanoparticles on Graphite, American Vacuum Society (AVS) 55th International Symposium, Boston (United States) 19-24, October, 2008.

5. Takahiro Kondo, Ken-ichi Izumi, Kenji Watahiki, June Pyo Oh, Daiichiro Sekiba, Hiroshi Kudo and Junji Nakamura, Catalytic property and morphology of Pt clusters on the graphite surface, 25th European Conference on Surface Science, Liverpool (United Kingdom) 8-12, July, 2008.

6. Takahiro Kondo, Ken-ichi Izumi, Kenji Watahiki, June Pyo Oh, Daiichiro Sekiba, Hiroshi Kudo and Junji Nakamura, Promoted Catalytic Activity of a Platinum Monolayer Cluster on Graphite, Pre-Symposium of 14th International Congress on Catalysis (ICC 14), Kyoto (Japan) 8-12, July, 2008.

7. Norikazu Kinoshita, Hiroshi Matsumura, Kotaro Bessho, Akihiro Toyoda, Kazuyoshi Masumoto, Yuki Matsushi, Kimikazu Sasa, Tsutomu Takahashi, Shozo Mihara, Toshiyuki Oki, Masumi Matsumura, Yuki Tosaki, Keisuke Sueki, Michiko Tamari, Yasuo Nagashima, Depth profile of radioactivity induced in the thick concrete shield in EP-1 beam line at the 12-GeV proton synchrotron facility, KEK. The 11th International Conference on Radiation Shielding (ICRS-11), April 13-18, 2008, Callaway Gardens, Pine Mountain, Georgia, USA.

8. Yuki TOSAKI, Norio TASE, Kimikazu SASA, Tsutomu TAKAHASHI, Yasuo NAGASHIMA, Estimation of groundwater residence time using bomb-produced ^{36}Cl: a case study on spring waters from Mt. Fuji, Japan, the 36th the International Association of Hydrogeologists (IAH) Congress 2008, "Integrating groundwater science and human well-being, 26 Oct. - 1 Nov. 2008, Toyama, Japan.

9. Kimikazu Sasa, Yuki Matsushi, Yuki Tosaki, Michiko Tamari, Tsutomu Takahashi, Keisuke Sueki, Shozo Mihara, Toshiyuki Oki, Yasuo Nagashima, Hiroshi Matsumura, Norikazu Kinoshita, Kotaro Bessho, Kazuho Horiuchi, Hiroyuki Matsuzaki, Yasuyuki Shibata, Motohiro Hirabayashi and Hideaki Motoyama, Cosmogenic nuclide ^{36}Cl measurements in the Dome Fuji ice core, Antarctica, The 11th International Conference on Accelerator Mass Spectrometry (AMS11), Rome, Italy, 14th to 19th September, 2008.

10. Kimikazu Sasa, Tsutomu Takahashi, Yuki Tosaki, Michiko Tamari, Keisuke Sueki, Toshiyuki Oki, Shozo Mihara, Yoshihiro Yamato, Yasuo Nagashima, Hiroshi Matsumura, Kotaro Bessho, Norikazu Kinoshita, Yuki Matsushi, Status and research programs of the multi-nuclide AMS system at the University of Tsukuba The 11th International Conference on Accelerator Mass Spectrometry (AMS11), Rome, Italy, 14th to 19th September, 2008.

11. Yuki Matsushi, Kimikazu Sasa, Tsutomu Takahashi, Keisuke Sueki, Yasuo Nagashima, Yukinori Matsukura, Chlorine-36 in calcite: denudation rates of karst landform in Japan, The 11th International Conference on Accelerator Mass Spectrometry (AMS11), Rome, Italy, 14th to 19th September, 2008.

12. Yuki Tosaki, Gudrun Massmann, Norio Tase, Kimikazu Sasa, Tsutomu Takahashi, Yuki Matsushi, Michiko Tamari, Yasuo Nagashima, Kotaro Bessho, Hiroshi Matsumura, Distribution of ^{36}Cl in groundwater: an attempt to estimate local fallout of bomb-produced ^{36}Cl, The 11th International Conference on Accelerator Mass Spectrometry (AMS11), Rome, Italy, 14th to 19th September, 2008.

13. Michiko Tamari, Keisuke Sueki, Yuki Tosaki, Yuki Matsushi, Toshiyuki Oki, Shozo Mihara, Norikazu Kinoshita, Hiroshi Matsumura, Kotaro Bessho, Tsutomu Takahashi, Kimikazu Sasa, Yasuo Nagashima, Chemical procedure of sulfur reduction for ^{36}Cl-AMS: A case of soil samples, The 11th International Conference on Accelerator Mass Spectrometry (AMS11), Rome, Italy, 14th to 19th September, 2008.

14. Silke Merchel, Wolfram Bremser, Vasily Alfimov, Maurice Arnold, Georges Aumatre, Lucilla Benedetti, Didier L. Bourl'es, Régis Braucher, Marc Caffee, Marcus Christl, L.Keith Fifield, Robert C. Finkel1, Stewart P.H.T. Freeman, Aarón Ruiz Gómez, Peter W. Kubik, Dylan H. Rood, Kimikazu Sasa, Peter Steier, Steve G. Tims, Anton Wallner, Klaus M. Wilcken, and Sheng Xu, Be-10 and Cl-36 interlaboratory comparisons, Annual Meeting of the DPG (DPG=German Physical Society) and DPG Spring Meeting of the Section AMOP, Hamburg, Germany from 2nd - 6th of March 2009.

7. THESES

Ph. D. Theses

Yuki Tosaki	Estimation of groundwater residence time using bomb-produced chlorine-36

M. Sc. Theses

Michiko Tamari	Analysis of long-life radionuclide Cl-36 in the soil by AMS
Mitsuteru Fujieda	Formation of condensation nuclei under proton irradiation
Masakuni Murakami	Precise measurement of energy losses of fast carbon clusters
Yuki Sato	Development of electrostatic ion beam trap

8. SEMINARS

Date		Title and *Speaker*
2009		
Jan	28	Study of Physics Performance of Transition Radiation Detector and D/B Mesons Identification Capability at LHC-ALICE Experiment *M. Sano (Univ. of Tsukuba)*
		Determinations of Reaction Plane and Back-to-Back Jet Axis at LHC- ALICE Experiment *D. Sakata (Univ. of Tsukuba)*
Mar	18	ANSTO AMS Facility and recent applications *Quan Hua (ANSTO)*
Mar	26	LHCf experiments and high energy cosmic rays *T. Sako (Univ. of Nagoya)*
Mar	26	Ions in the atmosphere - a link between the Sun and Earth's climate? *Jens Olaf Pepke Pedersen (National Space Institute, Danish Technical University)*

9. SYMPOSIUM

Annual meeting of UTTAC users

Ion-beam based interdisciplinary studies

16 March, 2009

Laboratory of Advanced Research B 0110

1. Opening : *H. Kudo (Uinv. of Tsukuba)*
2. Fabrication of ZnO nanoparticles by ion implantation and thermal oxidation : *H. Amekura (NIMS)*
3. Sharpening of gold nanoparticles in SiO_2 by bombardment of ion beam and the mechanism *K. Awazu (AIST)*
4. RBS study on degradation mechanism of swichable mirrors : *D. Sekiba (Univ. of Tsukuba)*
5. In situ observation of hydrogen by nuclear reaction analysis : *K. Fukutani (Tokyo Univ.)*
6. Applications of AMS for geoenvironmental science and Antarctic ice core : *K. Sasa (Univ. of Tsukuba)*
7. Analysis of radionuclide Cl-36 in the soil by AMS : *K. Sueki (Univ. of Tsukuba)*
8. Trace element analyses of fluid inclusions in quartz crystals from Tsushima granite with shallower emplacement level : *M. Kurosawa (Univ. of Tsukuba)*
9. Droplet formation in $N_2/H_2O/SO_2$ by proton beam irradiation : *S. Tomita (Univ. of Tsukuba)*
10. Application of NMR using unstable nuclei to the study of nuclear moments and material science : *M. Mihara (Osaka Univ.)*
11. Physics of unstable nuclei in UTTAC : *A. Ozawa (Univ. of Tsukuba)*
12. Study of nucleosynthesis by gamma-ray spectroscopy : *T. Komatsubara (Univ. of Tsukuba)*

10. LIST OF PERSONNEL

Tandem Accelerator Complex

H. Kudo	Director, Professor
T. Komatsubara	Assistant Professor
K. Sasa	Assistant Professor
D. Sekiba	Assistant Professor
S. Ishii	Mechanical Engineer
H. Kimura	Computer Engineer
H. Oshima	Electric Engineer
Y. Tajima	Mechanical Engineer
T. Takahashi	Electric Engineer
Y. Yamato	Electric Engineer
Y. Tagishi	Research Coordinator
H. Naramoto	Research Coordinator
S. Mihara	Research Fellow
T. Oki	Research Fellow
M. Moro	Administrative Stuff

Steering Committee

H. Kudo	Y. Miake	T. Sakae	K. Matsukura	K. Murakami
A. Ozawa	T. Komatsubara	K. Sasa	D. Sekiba	

Research Members [1]

Inst. of Physics

I. Arai	T. Komatsubara	M. Onoda	A. Ozawa	K. Sasa
Y. Yasuda				

Inst. of Applied Physics

S. Aoki	K. Akimoto	E. Kita	H. Kudo	T. Suemasu
S. Tomita	A. Uedono	H. Yanagihara		

Inst. of Materials Science

T. Kondo	J. Nakamura

Inst. of Engineering Mechanics and Systems

K. Matsuuchi

Inst. of Geoscience

M. Kurosawa	N. Tase	Y. Tosaki

[1] The "research members" include the authors and coauthors within 5 years back from this fiscal year, as well as the members of research projects runnning at UTTAC.

Inst. of Chemistry

K. Sueki

Graduate students

Doctoral Programs of Pure and Applied Science

M. Iijima	Y. Ikeda	K. Miki	T. Moriguchi	M. Shimomura
R. Tanabe	K. Watanabe	K. Yamaguchi		

Master's Programs of Pure and Applied Science

M. Fujieda	E. Hamada	M. Horikoshi	T. Ikuyama	Y. Ito
M. Kajigaya	M. Kimura	M. Matsuoka	M. Minakawa	M. Murakami
H. Nakamori	K. Ogawa	A. Oonishi	D. Sakata	M. Sano
Y. Sato	K. Shiba	N. Shiobara	M. Tamari	T. Todoroki
H. Yokoyama				

Undergraduates

S. Abe	T. Amano	Y. Ishibashi	T. Kayano	N. Kurihara
H. Ooishi	H. Satake	Y. Sekine	T. Takeuchi	K. Terada
T. Watanabe				

Scientific Guests and Fellows

K. Awazu	AIST
M. Fujimaki	AIST
S.J. Yu	Waseda Univ.
K. Sugimoto	Waseda Univ.
K. Nomura	Waseda Univ.
A. Maeda	Waseda Univ.
S. Fujii	Waseda Univ.
T. Kato	Waseda Univ.
K. Sato	Waseda Univ.
Y. Matsushi	Tokyo Univ.
H. Muramatsu	KEK
K. Bessho	KEK
K. Masumoto	KEK
N. Kinoshita	KEK
T. Miura	KEK
T. Hayakawa	JAEA
T. Shizuma	JAEA
H. Matsumoto	JAXA
T. Komiyama	JAXA
Y. Sasaki	JAXA
Y. Terakado	Meisei Denki
M. Nakazawa	Meisei Denki
M. Kusakabe	Meisei Denki
M. Tomitaka	Meisei Denki
H. Yamaguchi	AIST
T. Ooyanagi	AIST
Y. Ohura	Tokyo Metropolitan Univ.
H. Hashizume	Tokyo Metropolitan Univ.
Y. Hamanaka	Tokyo Metropolitan Univ.
S. Kubono	CNS
S. Hayakawa	CNS
D. Kahl	CNS
D.N. Binh	CNS
A. Chen	McMaster Univ.
J. Chen	McMaster Univ.
K. Hara	RIKEN